January 2012

Crack Analysis in Silicon Solar Cells

Maria Ines Echeverria Molina
University of South Florida, miecheverria@mail.usf.edu

Crack Analysis in Silicon Solar Cells

by

Maria Ines Echeverria Molina

A thesis submitted in partial fulfillment
of the requirements for the degree of
Master of Science in Materials Science and Engineering
Department of Mechanical Engineering
College of Engineering
University of South Florida

Co-Major Professor: Ashok Kumar, Ph.D.
Co-Major Professor: Sylvia Thomas, Ph.D.
Yusuf Emirov, Ph.D.
Rasim Guldiken, Ph.D.
Manoj Ram, Ph.D.

Date of Approval:
October 26, 2012

Keywords: Crack propagation, Crack depth, Crack location, Efficiency, FIB

Dedication

I lovingly dedicate this thesis to my parents, Felipe Echeverria and Ines Molina, and sisters for their constant support, love and encouragement throughout my life; for their daily talks of love and perseverance, and for taking care of me in the distance.

Acknowledgments

I would like to express my sincere gratitude to Dr. Yusuf Emirov for all his invaluable help and technical guidance, his teaching sessions and patience.

I would like to thank Dr. Kumar for his help and support throughout my masters' studies, and Dr.Manoj for his assistance in this project and technical guidance. Furthermore, thanks to Dr. Sylvia Thomas for her support, guidance, motivation, and enthusiasm, and Dr. Rasim Guldiken for his insightful comments and questions.

I am thankful to Dr. Ostapenko and Ultrasonich Technologies, Inc. for their support through grants from Department of Energy, and Florida High-tech Corridor. Likewise, I am grateful to the NREC staff, especially to Robert Tufts and Sclafani Louis-Jeune for their help and support.

Last but not the least I would like to extend my sincerest thanks to my professors at Universidad del Norte who were an important part in the process of me becoming a mechanical engineer.

Table of Contents

List of Tables

List of Figures

Abstract

Solar cell business has been very critical and challenging since more efficient and low costs materials are required to decrease the costs and to increase the production yield for the amount of electrical energy converted from the Sun's energy. The silicon-based solar cell has proven to be the most efficient and cost-effective photovoltaic industrial device. However, the production cost of the solar cell increases due to the presence of cracks (internal as well as external) in the silicon wafer. The cracks of the wafer are monitored while fabricating the solar cell but the present monitoring techniques are not sufficient when trying to improve the manufacturing process of the solar cells. Attempts are made to understand the location of the cracks in single crystal and polycrystalline silicon solar cells, and analyze the impact of such cracks in the performance of the cell through Scanning Acoustic Microscopy (SAM) and Photoluminescence (PL) based techniques.

The features of the solar cell based on single crystal and polycrystalline silicon through PL and SAM were investigated with focused ion beam (FIB) cross section and scanning electron microscopy (SEM). The results revealed that SAM could be a reliable method for visualization and understanding of cracks in the solar cells.

The efficiency of a solar cell was calculated using the current (I) - voltage (V) characteristics before and after cracking of the cell. The efficiency reduction ranging from 3.69% to 14.73% for single crystal, and polycrystalline samples highlighted the

importance of the use of crack monitoring techniques as well as imaging techniques. The aims of the research are to improve the manufacturing process of solar cells by locating and understanding the crack in single crystal and polycrystalline silicon based devices.

Chapter 1: Introduction and Background

1.1 Scope and Motivation

Currently, main sources of energy are limited by fossil fuel based energy. This kind of energy is non-renewable, expensive and takes a very long time to form. The extraction of fossil fuels leads contamination affecting not only human beings but all living beings, sea and land ecosystems. These facts are leading the drive for new sources of clean and renewable energies. Sun, water, wind and bio-fuel have been investigated and implemented as new sources of power supply but research is still necessary to increase efficiency of energy conversion as well as to reduce costs to make them more economic feasible.

Solar energy has been attractive because of the high ratio between the lifetime of a solar panel and the emission of contaminants from the production process. This source of energy can be produced locally which reduces the costs of energy distribution. Researchers have studied different materials suitable for this application, but again, the cost of production is an issue as well as the efficiency. In this matter, countries are looking forward to renewable energies that will reduce the dependence on fossil fuels, satisfy the needs of population and diminish the impact of an energy crisis by increasing the production yield and decreasing production costs.

The main objective of this research project is to identify cracks in monocrystalline and polycrystalline silicon solar cells by finding a reliable imaging technique for this purpose and analyzing the impact of cracks in the performance of the cells.

1.1.1 Outline

This chapter provides the background on solar cell principles, materials for solar cells, manufacturing processes for silicon and solar cells, imaging techniques and two microscopy techniques used in this research. The second chapter corresponds to the description of materials, tools and set-up used to make the experiments to accomplish our objective. Details about the solar cells utilized, imaging techniques employed such as Photoluminescence (PL), Scanning Acoustic Microscope (SAM), Scanning Electron Microscope (SEM) and Focused Ion Beam (FIB) system; and equipment for characteristic voltage and current measurements were included to ensure repeatability of the experiments.

Chapter 3 presents the findings of this research. Images from PL and SAM are shown as part of the comparison between the two techniques. Ions and electron stimulated SEM images are presented as part of the confirmation of the existence of the cracks, and analysis of the solar cell composition layers. Finally I-V curves before and after cracking are shown to calculate the efficiency reduction of the cell due to the crack induced. Lastly, chapter 4 presents conclusion and recommendation to the results obtained and future work.

1.2 Solar Cells

Solar cells work using the photovoltaic (PV) effect. Even though the solar cells have been available since the 50's, research in photovoltaic effect started on 1839 [1]. This effect was first seen in Selenium which was used for many years in application of low energy requirement. After a deeper understanding of the principles of the effect by Albert Einstein and Schottky, there were efficient solar cells made and some were used in satellites [2].

The PV energy conversion is done in the cell in two steps: the first one is related to the generation of electron-hole pairs by absorption of light; and the other step is related to the separation of electron and holes by the structure of the device. Electrons go to the negative terminal (n-doped material) and holes to the positive one (p-doped material) [3]. At the junction of both types of material, a phenomenon called depletion takes place. This phenomenon occurs in the junction after electrons have joined the holes; when there are no more carriers available in the zone and extra carriers outside the zone are not allowed to join together [3].

The p-n junction known as diode structure makes electrons to flow just in one direction and it has an electric field associated to it. This direction limitation allows electrons to pair holes just by passing through an external circuit, placed outside the device. This process produces a current from the solar cells while they are lighted by the sun [3]. The following image shows the structure of a solar cell that allows for the phenomenon briefly described above.

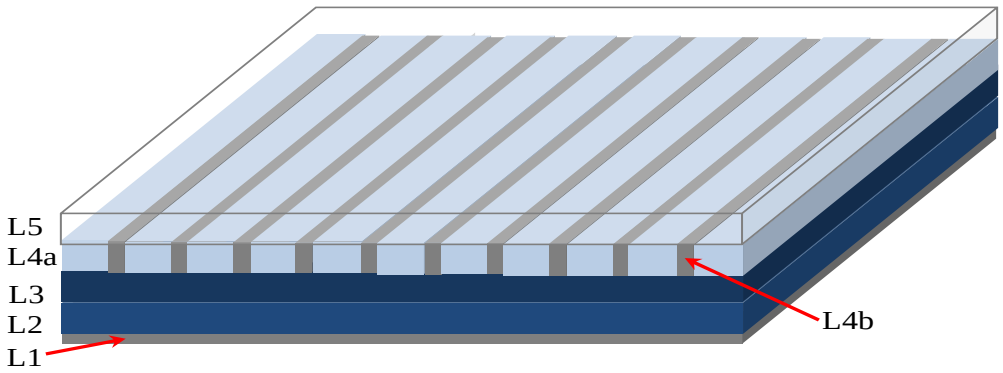

Figure 1. Schematic structure of a solar cell [4].

The first layer (L1 as shown in Figure 1) is the back contact. This layer is placed at the back of the device and is made of metallic materials acting as a conductor. The second layer (L2) is a p-type material; the base material is doped with another material which has one less valence electron than the base (boron in the silicon case), that lets an incomplete bond that attracts electrons from other base material atoms [3]. The third layer (L3) represents the n-type material, in this case the material is doped with another material with one more valence electron (phosphorous or arsenide in the silicon case). The extra electron is available for conduction. After the Silicon is doped a contact grid is made on its surface (L4b). This grid is made of metal and serves also as conductor collecting electrons [4].

Once the contact grid is made an antireflective coating is applied on the surface of the cell (L4a), usually silicon oxide, silicon nitride or some texture (cones and pyramid made by etching) are used. This coating is designed selecting the right thickness and refractive index based on the Snell's Law. The antireflective layer serves as guide for the incident light to the solar cell. The last layer (L5) is called encapsulate. This layer helps to reduce the influence of the environmental condition on the cell. It is usually made of glass or clear polymers [4].

1.2.1 Manufacturing Process

The process to manufacture solar cells starts with ingots of a PV material; this ingot has a circular cross section and is cut first to make it semi-square shaped and then sliced to create wafers [5]. The wafers are polished to reduce surface damage from slicing process. Then they are p-doped and n-doped by introducing impurity atoms to the structure. Different doping techniques can be used such as vapor deposition, diffusion and ion implantation [5].

The contacts are usually made of aluminum or other metals which could be deposited by evaporation or sputtering [6]. The front grid contact manufacturing is usually made by photolithography process that consists of: a) application and spinning of a photoresist; b) soft baking to dry and improve adhesion of resist over the surface; c) exposure of pattern mask over the resist with UV light; d) developing and etching of exposed aluminum using an acid solution; e) removal of remaining photoresist. The back contact is made after the front grid contact litho process. Another materials used are aluminum paste or metallic paste for which the process used to deposit the contacts is called screen-printing. In this process the metallic paste is printed wet all over the rear surface and grid printed on the front surface. A highly p-doped layer called back surface field is added before printing to reduce electron-hole recombination [7].

Either of those processes induces residual stresses due to the difference in thermal expansion coefficient and mechanical behavior between silicon and the metallic paste. Bowing of the cell is a big problem that come after cooling and may cause cracking and fracture [8].

The antireflection coatings are applied and spun to ensure a constant thickness through the surface of the wafer; parameters as spin speed and spin time depend on the material selected as coating and the thickness required. Finally the wafer is annealed to create an ohmic contact between the base material and contacts [5].

1.2.2 Performance of Solar Cells

The performance of a solar cell is determined by the amount of energy that the device can transform into electric energy [9]. This amount of energy depends on the quality of the material (type and area); and the sun light intensity and wavelength. The output energy of the solar cell is almost directly proportional to the light intensity and cell area. A higher intensity of sunlight will let a higher energy as well as a higher area will let a higher energy. Furthermore the voltage in the cell does not depend on its size and is almost constant to changes in light intensity [9].

Other factors that influence the performance of the solar cells are the reflection, since some of the photons that hit the cell do not penetrate it but are reflected; low energy photons that do not debond the electrons from the atoms, avoiding generation of electron-hole pairs [9]. Also high recombination since some electron-holes pairs generated does not reach the external field, losing energy and reoccupying the energy state they had before in the valence band. Another factor that should be mentioned is the parasitic resistance. This is explained by the manufacturing process that fuses the silicon and the aluminum contacts being that some remaining space is still in the interface increasing the

resistance and reducing the power transferred to the load [10]. This fact explains very well the effect of cracking in the solar cells.

As an example of the influence of the factors mentioned above, the following table show a comparison between different types of silicon solar cells.

Table 1. Comparison between different types of silicon.

Type of material	Maximum efficiency	Limitations
Monocrystalline Si	≤25%	Complexity and high cost of manufacturing. Highly sensitive to impurities.
Polycrystalline Si	<20%	Internal energy losses higher than in monocrystalline silicon due to imperfections and impurities within the crystal [11]
Amorphous Si	≤10%	Initial deterioration, stability over time

Because of the relatively low efficiency of energy conversion of solar cells there is necessary to make arrays of cells called solar modules, which increment the cost of this type of energy. The efficiency of a solar cell can be also increased by the use of concentrators that allows for concentration of sunlight in the cell; and the use of solar trackers that let to track the motion of the sun across the sky to ensure that the maximum amount of sunlight hit the cells when it is available [9]. There are some limitations in this matter because of the complexity of the mechanisms used and the high temperatures reached within the cell which makes necessary to implement a cooling system. Different approaches for cooling systems have been presented, such as heat pipe using water or acetone as the working fluid for passively cooling concentrator solar cells operating up to 500suns [12] or de-ionized water immersion cooling [13].

1.2.2.1 Electrical Characteristics of Solar Cells

There are three variables that define the electrical characteristic of the solar cells in terms of the voltage-current (I-V) characteristic curves: intensity of the solar radiation, temperature and area of the cell. The first term has no major effect on the open circuit voltage (Voc) but has a significant influence in the intensity of the short circuit current (Isc), increasing as it increases [10]. On the other hand, the temperature affects the reading of the Voc as temperature increases Voc decreases; and does not affect significantly the Isc. The cell area makes the Isc increase as it increases and has no major effect in Voc [10]. Table 2 summarizes this statement. Isc and Voc are maximized in closed-circuit and in open-circuit conditions respectively. This both conditions represent no power generation, in other cases the power will increase while voltage is increasing until it reaches a maximum and decreasing rapidly close to Voc.

Table 2. Factors influencing characteristic parameters of a solar cell.

Variable	Influence in characteristic parameter	
	Voc	Isc
Intensity of solar radiation	No significant effect	Directly proportional
Temperature	Inversely proportional	No significant effect
Area of the cell	No significant effect	Directly proportional

Other common parameters that are used to define solar cells are the fill factor (FF) and the efficiency. The fill factor is a measurement of the "squareness" of the performance of the solar cell (I-V curve) and is defined as the ratio of the maximum power and the area of a rectangle formed by Voc and Isc. The efficiency (η) of the cell is defined as the ratio of the power it generates and the maximum optical power incident on

the cell. The incident optical power is understood as the maximum solar power incident on the earth surface and is usually given in W/m^2 [14]. The efficiency and the full fill factor are given by the equations below

$$FF = \frac{I_{max}V_{max}}{I_{SC}V_{OC}} \qquad \text{[15] Equation 1}$$

$$\eta = \frac{P_{max}}{P_{in}} = \frac{V_{OC} * I_{SC} * FF}{P_{in}} \qquad \text{[15] Equation 2}$$

where Imax and Vmax are the maximum cell current and voltage respectively at the maximum power point and Pin is the power input to the cell. The figure below shows the output current and power of a solar cell as function of the voltage; the area A and B represent the numerator and denominator of the fill factor equation.

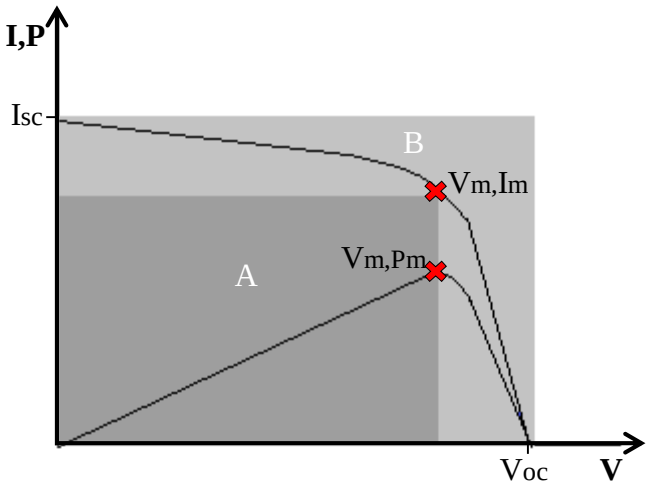

Figure 2. Characteristic output curve of a solar cell [16].

Solar cells have an equivalent circuit model that consists of a current source (photon source); a diode (the cell itself); a series resistance that symbolize the ohmic

losses in the front surface of the cell; and a shunt resistance corresponding to the losses due to diode leakage current [17]. The series resistance influence the performance of the cell decreasing the voltage of maximum power point resulting in decrement of efficiency [18] and the shunt resistance might affect the cell power output indicating defective manufacturing processes and trustworthiness issues [19]. Both parameters are also affected by the incident light which is the input power, it has been found that there is an increment of the shunt resistance when the input power increases until a stable value is reached; on the other hand, there is always a decrement of the series resistance when increasing input power. However, the rate of decrease increases at lower input power values [20].

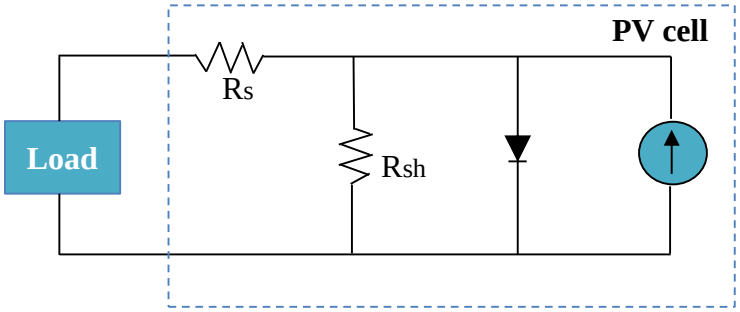

Figure 3. Equivalent circuit of a photovoltaic cell [16].

1.2.2.2 Cracks in Silicon Solar Cells

Crack formation in solar cells is related to the mechanical strength of the material as well as the processing necessary to manufacture the cells [21]. The overall strength of the wafer is known to be associated to the size, density and distribution of defects [22]. In order to obtain the cell with required size, the processing plays a significant role since it could induce cracks and posterior breakage of the cell reducing the production yield and increasing the production costs.

Steps that could induce cracks during the manufacturing process include sawing and cutting of the silicon ingot or brick, deposition of the conductive contact films, wafer annealing, soldering of contacts on the cell surface, and mounting of cells to create solar modules [23]. As example, it has been found that the Aluminum back layer affects the mechanical behavior of the cell; increasing the bending strength of the silicon solar cell but it is remarkable that this fact depends on parameters as thickness, porosity, concentration of bismuth glass, and thickness of the eutectic layer; this latter increases fracture strength by inducing plasticity on the cell [22]. In the particular case of polycrystalline silicon solar cells is known that the fracture strength is extremely linked to intrinsic properties of the material as grain size and boundaries, as well as crystal orientation; and features like flaws and micro-cracks [22].

The efficiency of the solar cell is influenced by the overall manufacturing process. Cracks and other defects represent a decrement in conductivity letting location zone disconnected or inactive for electric purposes which means a loss in power output and drop of efficiency [24] [25].

1.3 Materials for Solar Cells

Researchers all over the world are studying different materials usable in photovoltaic cells. Some authors have analyzed abundant, non- toxic binary potential materials [26] where materials other than the conventional Silicon (Si), cadmium telluride (CdTe), and copper-indium-gallium selenide Cu(In,Ga)Se_2 (CIGS) are examined. Other authors [27] have talked about the use of chemically deposited lead sulfide and bismuth

sulfide thin films and (Bi_2S_3/PbS) as potential materials since they have the requirements necessary for working as photovoltaic layer in the solar cell. These authors foresee a substantial increase in efficiency while decreasing the cost of manufacturing.

In addition other authors have been studying the use of organic materials such as organic polymers, pigments and dyes, polymers and the hybrid organic-inorganic solar cell [28] [29] even though these materials let low efficiency solar cell, they are highly versatile and allow for changing in properties as band gap; and have the potential of low cost, lightweight and environmentally friendly devices [30].

Despite there are many materials that have been studied for this application, gallium arsenide and silicon are the most used materials for this application because of the high efficiencies reached. Gallium arsenide is more expensive than silicon and is created especially for PV use while the silicon being one of the materials more abundant on Earth is available in ingots made for microelectronic fabrication industry. The silicon wafer contributes about 75% of the overall cost of the solar cell [31]; to reduce manufacturing costs the silicon wafers have been sliced thinner and the area has also been increased.

1.3.1 Silicon for Solar Cells

Silicon is obtained from quartzite reduction with carbon in an arc furnace [32]. The product of this process is called metallurgic grade silicon which has about 98% purity. This material is not pure enough for microelectronics fabrication so a process of refraction is due to improve quality. The milled metallurgic silicon is exposed to

hydrochloric gas in a fluidized-bed reactor. The reaction is given by $Si+3HCl \rightarrow SiHCl_3+H_2$, where the hydrogen is taken away at temperatures below of 30C at which the trichlorosilane is liquid. The trichlorosilane is used and the chlorides are separated using distillation columns, at the end of the process the silicon is highly pure [32].

Crystalline silicon has a diamond cubic structure acting as a brittle material. It has four valence electrons and is one of the most used semiconductors with controllable conductivity in the range of 0.02-1000 $(\Omega cm)^{-1}$.

Defects in silicon have an influence in the performance of the devices. Some defects are vital but others fatal. For the semiconductor industry controlled substitution is essential for a good performance however a high addition of elements let the material useless. These defects can be zero-dimensional or point defects such as vacancy, interstitial and Frenkel defects; One dimensional or line defects for example straight dislocations and loops; They can also be two-dimensional or area defects as grain boundaries and fault stacking order; as well as three-dimensional or volume defects such as voids and precipitates of point defects. Each type of defect gives different properties to the material affecting the functioning of the device. The grade of perfection of the silicon and amount of impurities affect the lifetime of minority charge carrier although structural defects can operate as recombination spots [33]. Hence, dislocations produce adverse effects acting as a sink for the doping impurities and interfering with diffusion profile.

There are different alternatives for solar cells when the material selected is silicon. Depending on the fabrication process the silicon ingot can grow crystalline or

amorphous and each one has different characteristics and advantages that make them suitable for this application.

1.3.1.1 Monocrystalline Silicon

Crystalline materials can grow either monocrystalline or polycrystalline according to the technique implemented. Monocrystalline silicon are created using methods such as Czochralski, Float-Zone and Ribbon-Growth. The most common method to grow monocrystalline silicon is the Czochralski (CZ) method. This technique consists in melting pure polycrystalline silicon in a quartz crucible and pull up a monocrystalline seed at controlled temperature, rotation speed and pull-up speed. The seed has the required crystal orientation. A small amount of p-type doping material can be added to the molten silicon to create p-doped silicon [34].

This method is well known because of its low cost and simplicity but the purity of the single crystal is lowered due to impurities than come from the crucible and oxygen that may lead to a decrement in the lifetime of the cell; these parameters have to be also controlled [32]. The silicon used is a mix of virgin polycrystalline silicon and wasted material from the microelectronic industry which allows reducing costs. One of the main disadvantages of this method is the circular ingot shape. With the purpose of building an efficient solar cell is necessary to cut the ingots into pseudosquare shape [35]; this step leaves scrap silicon behind. Besides the tail and top of the ingot are not usable, all of the material wasted in the production line can be reused mixing it with virgin polycrystalline silicon. Scrap materials from the microelectronic industry are also utilized.

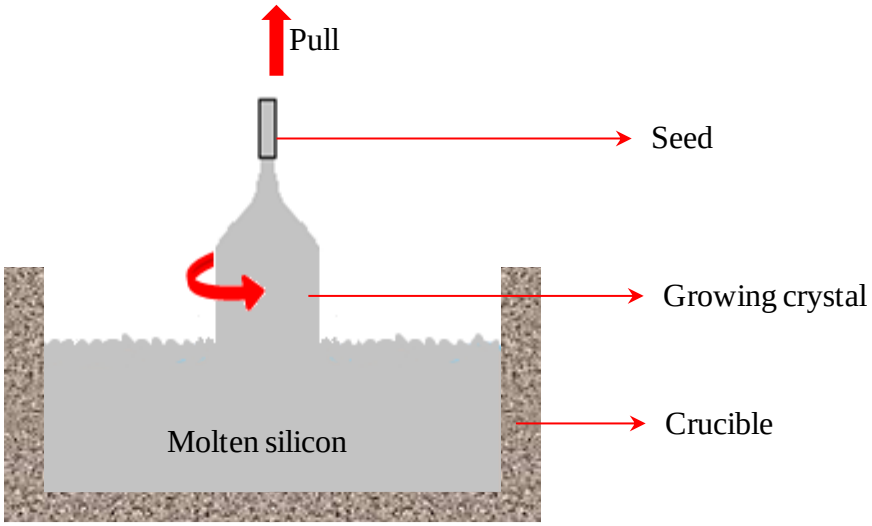

Figure 4. Schematic of Czochralski growth [34].

The float zone (FZ) method consists of pushing a polycrystalline rod through a heating coil that melts the silicon; in the opposite side there is a pure monocrystalline seed of silicon pulling the molten silicon. This is done in the presence of an inert gas. As in the CZ method, parameters such as temperature, rotational speed and linear speed have to be carefully controlled to ensure the required quality. It is possible to get doped silicon from this method by adding a dopant gas such as phosphine (PH_3) or diborane (B_2H_6) to the inert gas [32]. This technique lets a high purity monocrystalline ingot since there is no crucible and contact between materials except for the seed [34]. Furthermore, this monocrystalline structure is highly perfect because it does not contain volume defects, planar or linear defects.

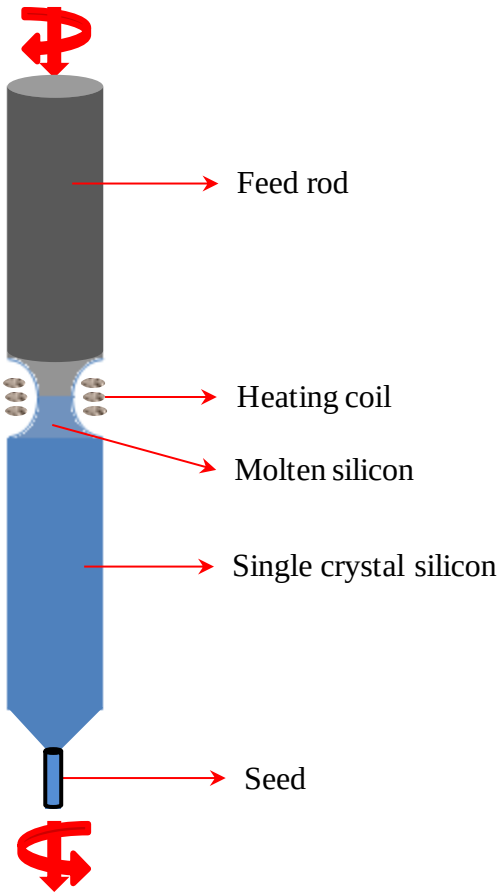

Figure 5. Schematic of float zone growing method [34].

1.3.1.2 Polycrystalline Silicon

The production of polycrystalline silicon is easier than the monocrystalline version reducing the costs of manufacturing but also the efficiency. One of the main advantages is the fact that it is no necessary an extra cutting step of the sides because of the square/rectangular shape that can be achieved. The most used methods for obtaining multicrystalline silicon are block-casting, Bridgman process and ribbon growth [35].

Block casting and Bridgman methods are similar but differ in the number of crucibles needed. While for Bridgman process just one crucible is necessary for melting and crystallization; for block casting each of the steps is done in a different crucible.

Crucibles for Bridgman are made of silicon nitride-coated quartz that prevents silicon to adhere to the walls of the crucible. The crucible is destroyed due to the change in volume during the solidification process. This method uses induction heat to melt the silicon and the crystallization is carried out while moving downwards the crucible out of the heating compartment [35]. In the block-casting process the silicon is melted in an uncoated quartz crucible and then transferred to a silicon nitride coated crucible for the crystallization process. This method uses heaters to melt the silicon and controls the crystallization rate by regulating the temperature in the heater [35].

Crystallization process begins from the bottom of the crucible and goes upwards producing a columnar growth. In this process, the solidification speed plays a very important role because it influences the grain size [36], defect formations and thermal gradients resulting in cracks and even ruptures of the block. Speeds of about 1cm/h are common in the Bridgman method but for the block casting higher speeds are reached [35].

The Ribbon-growth technique is a group of methods created to avoid the necessity for slice the ingot to get the wafer. It consists basically of the continuous production of a thin sheet from the melted silicon; diverse techniques are used to establish the edges of the ribbons [34]. They were created at research and development (R&D) projects in different companies and in this moment just few of them are used in mass production and the most known are edge-defined film edge growth (EFG), string ribbon (SR) and dendritic web technology (WEB). EFG and SR produce large grain ribbons [35].

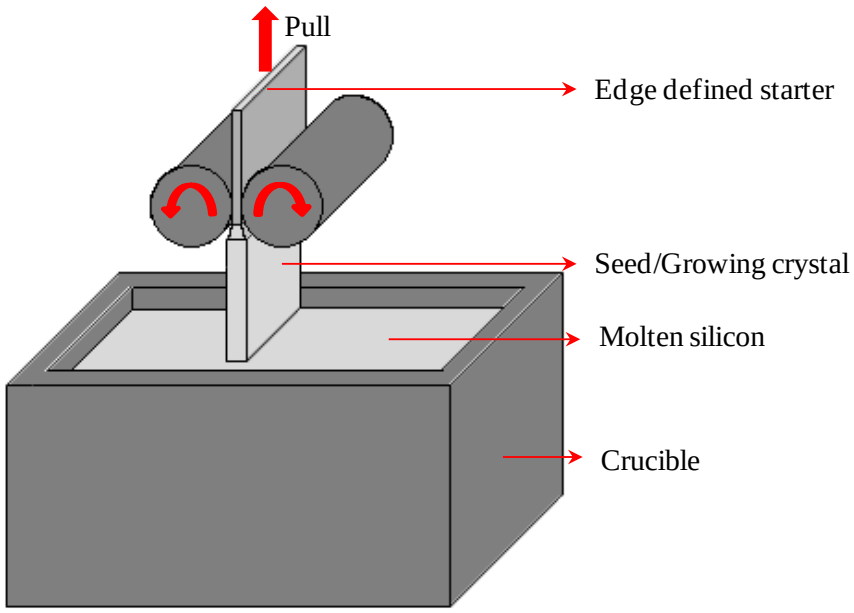

Figure 6. Schematic of EFG [37].

1.3.1.3 Amorphous Silicon

Amorphous silicon is fabricated by deposition of silicon in presence of silane (SiH_4) gas using 'glow discharges' (plasma deposition) or evaporation [38]. The electrical properties are fairly good but better for plasma deposited amorphous silicon. These properties can be improved by doping the thin film by mixing the silane with diborane (B_2H_6) or phosphine (PH_3) gas creating p-doped and n-doped amorphous silicon.

Research has been done to improve properties of amorphous silicon. Optoelectric properties, for example, has been enhanced by bonding hydrogen to the plasma deposited silicon [38]. This new structure is called hydrogenated amorphous silicon (a-Si:H). The amorphous silicon is attractive due to its relatively low cost and simple, as well as its capability to be used as solar cell but the efficiency is still low (<10%) compared to the crystalline versions.

1.4 Non-Destructive Techniques for Crack Detection in Solar Cells

Defects and excessive stress in the manufacturing process can cause cracks in the cell. These cracks diminish the performance of the solar cell by producing an inactive zone in the cell decreasing the efficiency of cells and modules. This is the reason why solar cell manufacturers have introduced in-line tools to detect cracks and other defects.

To match the throughput production is necessary to use reliable and fast methods to reject unviable wafers and increase the overall efficiency of the production. Hence different methods have been investigated to be useful in this aim, and different approaches can be implemented to get diverse results.

1.4.1 Resonance Ultrasonic Vibrations

The resonance ultrasonic vibration (RUV) method is one of the most used techniques to reject cracked wafers. Its use relies on the deviation of the response of a cracked silicon wafer or solar cell respect to an identical un-cracked version [39].

A piezoelectric transducer emits ultrasonic vibrations that produce acoustic waves that makes vibrate the wafer or cell and a system record and convert the response to a peak in a graph of amplitude versus frequency. The peak response depends on the size, geometry and material characteristics. A cracked wafer or cell shows a shift in frequency of the peak position, increment in the bandwidth and reduction of the amplitude signal [40].

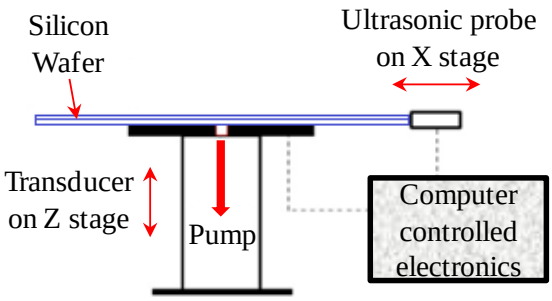

Figure 7. Schematic RUV set-up [41].

This method presents some limitations in response to ultrasonic vibrations for identical wafer which leads to the rejection of un-cracked wafer. To minimize this problem, statistical approach has been implemented and its validity has been verified [31] leading a widely used method because of its liability and the fact that it is not affected by scratches and other flaws which make it a fast in-line diagnosis method (< 2seconds per wafer/cell) . This technique doesn't reveal the crack position it is just used for rejection of cracked wafers or cells.

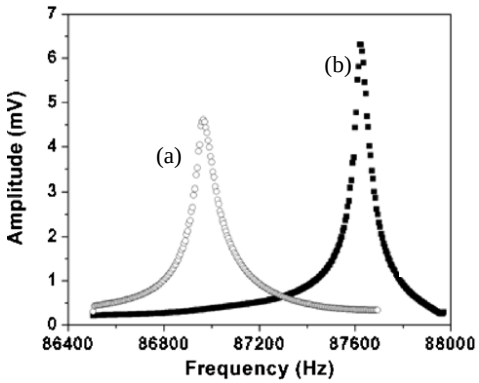

Figure 8. RUV response of (a) a cracked wafer and (b) a non-cracked wafer [40].

The sensitivity of the method was investigated by analyzing the relationship of crack location and vibration modes; results showed that some vibration modes are more sensitive to some crack locations confirming that any cracks located in the wafer can be identified by monitoring the vibration modes in RUV [40].

RUV has been studied for other applications. It is also used for diagnosis of elastic stress in silicon wafers, where particular vibration modes were recognized in wafers and associated to in-plane residual stress finding that the higher residual stress the higher the frequency of the vibration mode [41]. Besides the residual stress contained in wafers, because of manufacturing process, elastic stress due to the handling of the solar cells is also studied with RUV with the aim of minimize it and decrease the chance of breakage in subsequent process steps. Different vacuum holders were tested and analyzed and as a result a redesigned holder was optimized to diminish the influence of the handling stress in the capabilities of the RUV system [42]. RUV is also capable of detect pinholes in silicon solar cells when used with an Activation Station (AS) set up with information about the cell characteristics [43] [44].

1.4.2 Scanning Acoustic Microscopy

This technique uses a piezoelectric transducer that emits ultrasound or high frequency waves (>20 KHz). A coupling medium is used to diminish the reflection of the ultrasound, water or another not gaseous fluid can act as a good coupling between the sample and the transducer. These waves interact with the object and are scattered, absorbed or reflected by the features of the material as voids, cracks and delaminated surfaces [45].

Ultrasound principles have been used for different fields of knowledge; for example, in military with the use of the sonar, as well as in medicine with the implementation of sonography as a diagnostic imaging method for the human and

animal's body, and in industrial field to find flaws and measuring thickness of parts. Features with different acoustic properties are recognized as acoustic interfaces which are measured in terms of acoustic impedance. The acoustic impedance is given by

$$Z=\rho*c \qquad [46] \quad \text{Equation 3}$$

where rho is the density of the medium and c is the sound's velocity in the medium.

The change in acoustic impedance leads to reflection of part of the incoming ultrasound and transmission of remaining portion. The percentage amount of transmission (T) and reflection (R) from one medium to another is given by the expressions below

$$T = \frac{2(Z_1)}{(Z_1 + Z_2)} \qquad R = \frac{(Z2 - Z1)}{(Z2 + Z1)} \qquad [46] \quad \text{Equation 4}$$

where Z1 and Z2 are the acoustic impedances of the objects the ultrasound is going through.

The emission/receiver system can be pulse-echo-one transducer or through transmission; the first is the most used type in which just one transducer is used as emitter and receiver of the reflected beam, it can reveal which interface has openings with high spatial resolution [46]. The second uses two transducers, one to emit the ultrasonic wave and other below the sample to capture the transmitted beam through the sample; it can show openings at all interfaces but not which one has them [46].

The transducer can scan the back surface in a C-mode scanning of the sample but interfaces (top, back side of the wafer, walls of the container) can also reflect the ultrasonic pulses recorded by the ultrasonic detector. To avoid this signal a gate with data

from A-mode can be adjusted to the depth of interest. The mechanical scanning is done line by line by detecting the difference in impedance of the signals at the ultrasound boundaries, in this vein high reflectance takes place when the wave goes from a material with low impedance to one with large impedance or vice versa. A 2D image can be obtained by computing the amplitude and the phase of the reflected pulses [46].

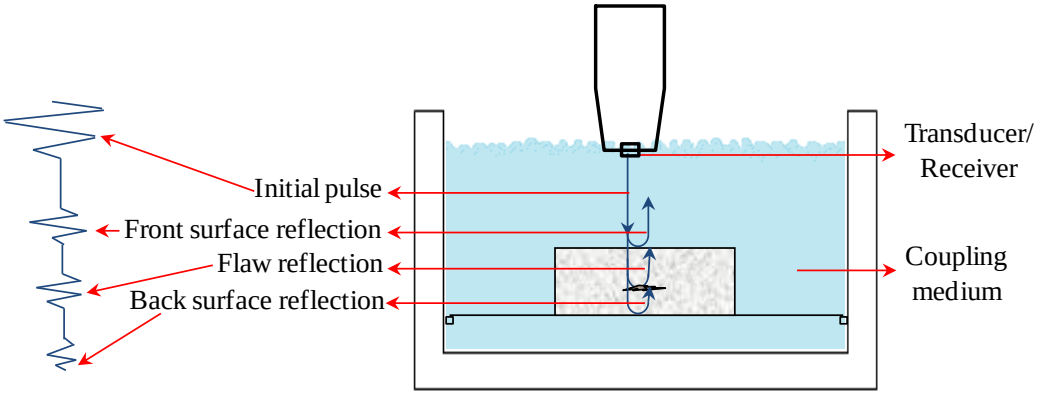

Figure 9. Schematic of a SAM system [46].

This technique has a resolution of about 1mm and takes about 20 min for set up and data collection which makes it not suitable as an in-line production step, but very useful for quantitative analysis, and calibration and validation of other millimeter-crack detection methods [47] [48].

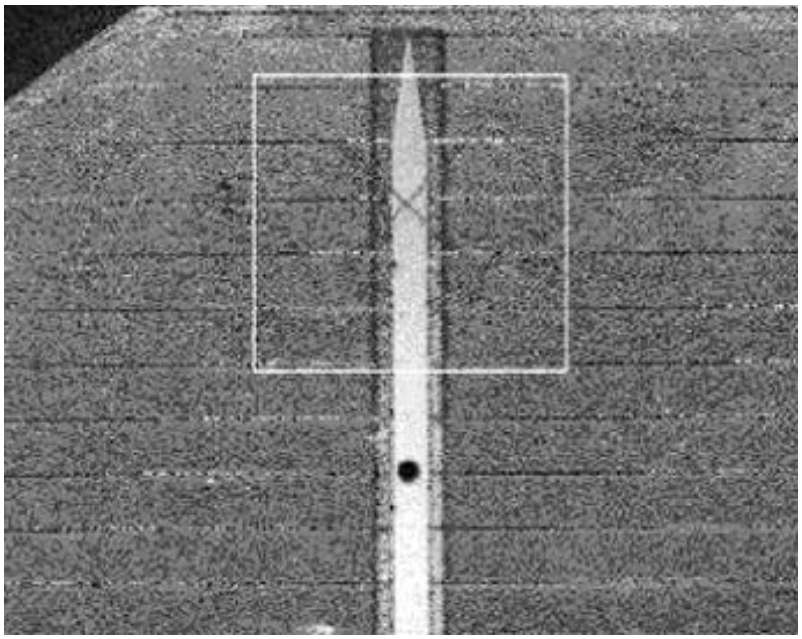

Figure 10. Scanning acoustic microscopy image of a crack in a silicon solar cell.

1.4.3 Electroluminescence and Photoluminescence Imaging Techniques

Luminescence techniques work using the principle of light emission of materials. The sample is exposed to an external energy that is absorbed and allows for the material to emit light at different wavelengths and the image is gotten by a CCD camera. Depending on the external energy applied luminescence can be of different types such as electroluminescence (EL) which uses electric field to excite the material; photoluminescence (PL) that uses an external light, mechanoluminescence which uses ultrasound or other means; or cathode luminescence (CL) that uses an electron beam to stimulate the material of the sample.

These methods rely on the fact that electron-hole recombination produces the emission of photons; the opposite process occurs in photovoltaics when due to exposure of photons, electrons from the valence band can jump to the conduction band.

Electroluminescence is a process in which electrons are excited by an electric current or electric field that leads to the recombination of electrons-holes. Energized electrons liberate the energy in form of photons that are imaged by a CCD camera. The wavelength of these photons for silicon can be in the range of 950-1250nm with a peak located at 1150nm. The amount of excitation depends on the defects density in the solar cell, for example a sample with many defects will emit less photons than a sample with few defects; thus the amount of light emitted is directly dependent to the induced current [49].

This method requires a complete processed module since contact is necessary to apply the electric current; therefore some mechanical damage can occur. Different features can be imaged by this technique including defects, impurity dislocations, surface features, cracks and grain boundaries [50]. Its capabilities allow for measurement with a high reproducibility but recombination that is carried out at grain boundaries results in decrement of the minority carrier life causing misleading of cracks with grain boundaries [51].

Photoluminescence is a process in which the material absorbs and emits photons; photons make electrons to jump from a lower energy state to a higher state, and then photons are re-radiated, letting electrons to go back to the lower state. The wavelength of these photons can be about 380-760nm (visible radiation) or 10-400nm (UV radiation). Since this process is done by optical excitation this technique can be used for application such as brick, as-cut wafers and partially processed cells reducing the mechanical damage due to contact with the sample, as is the case in EL [52].

The grade of excitation is related to physical characteristics of the materials such as electron-hole density, minority carrier lifetime, splitting of quasi-Fermi energy, defects and diode voltage. PL allows for computation and imaging of the sample showing a measure of these quantities; hence is a potential tool for cell performance study [52].

Therefore PL has been used to check the quality of an as-cut wafer before it enters to the solar cell fabrication process. Results show that grain boundaries are brighter for low quality multi-silicon wafer because of the gathering of impurities in the borders of the grains which means that high impurity density results in higher effective lifetimes. Dark spots represent bulk minority carrier lifetimes of <10 μs [53]. The response of the material depends on the temperature resulting in shift in the energy peak of the defect band and confirming the dependence of the silicon band gap to temperature; at room temperature the peak was in 0.77eV and as temperature was decreased band-to-band and defect band shifted to higher energies [33].

Although luminescence techniques are versatile, prompt and useful; defects such as scratches and dislocations interfere with the imaging of cracks and delamination. Preceding research in this topic showed that photoluminescence can show misleading cracks and surface scratches even though it has high spatial resolution [54] [55] [56].

1.4.4 Lock-in Ultrasound Thermography

Lock-in thermography techniques rely on the coded heat flow emitted by materials when exposed to periodic or sinusoidal high energy waves [57]. In other words, those techniques analyze the temperature modulation induced by the periodical heat

deposition. In ultrasound lock-in thermography (ULT), the material is heated by ultrasound adsorption due to the mechanical loss angle effect. The mechanical loss angle represents the phase angle by which strain lags stress in sinusoidal loading. The tangent of the angle usually describes the effect as the ratio between a real quantity, which is the conservative Young's modulus that occurs according to the deformation phase; and an imaginary quantity which is the loss modulus, displaced at some angle [57].

The thermal waves emitted due to ultrasound absorption are reflected by the boundaries of the sample; when reflected waves are superimposed to the initial wave, a change in signal or modulation frequency is caused; this change is correlated with the penetration depth [57]. The transducer is coupled into the sample and the ultrasound is modulated at low frequency; this produces a high hysteresis loss resulting in high heating at the defect location; this thermal wave is detected at the surface and the image is formed pixel by pixel analysis of the magnitude or phase of the modulated response [57].

This technique is not suitable for surface topography imaging and optical surface features recognition but because of its large depth range can be used to detect cracks, corrosion, impact damages, delamination of sandwich structures or coatings, and to measure thickness [58] [59].

1.5 Materials Investigation and Cross-Sectioning Technique

There are several tools available for materials investigation, such as microscopes with a resolution ranging from 350nm (optical) to 0.2nm (electrons transmission). Depending on the features and characteristics of the material one technique could be

more suitable than another one for a specific application. Light, electrons, ultrasound, and ions can be used to get an image of the surface and other relevant information from the materials with the aim of characterizes it.

1.5.1 Scanning Electron Microscopy

The scanning electron microscope is the most extensively used electron microscope because of its high resolution and depth of field capabilities, which allows to obtain images of the sample's surface with a 3D-appearance and to get chemical composition if possible [60].

The electron beam is created by an electron gun (thermionic or field emission type) and is passed through lenses of electromagnetic nature and apertures that decreases the diameter of the beam (condenser lenses), focus the beam on the surface of the sample (objective lenses) and diverge the beam in its path. The beam is deflected by two pairs of electromagnetic coils allowing the probe for moving along a line in the surface and changing the location to a next one to scan a new line [60].

When electrons hit the sample, secondary and backscattered electrons are created and x-rays are emitted. The secondary electrons (SE) are electrons that were ejected from atoms on the sample due to inelastic scattering, while the backscattered electrons (BSE) are incident electrons that were ejected from the sample due to elastic scattering. BSE are deflected at high angles with almost the incident energy and the latter are deflected at low angles with low energy compared to the BSE. The penetration of the beam and the

amount of electrons ejected from the sample are related to the atomic number of the material and other parameters [60].

Figure 11 and Figure 12 show the result of hitting a specimen with a high energy beam. Here it can be noticed that the electron beam penetrates deeply and with higher velocity in the carbon sample than in the gold one. The gold sample showed a concentrated penetration -and low backscattered electrons- zone which means that electrons from the beam are absorbed by the dense cloud of electrons form the sample. In the Carbon sample more electrons penetrate the sample as well as backscatter.

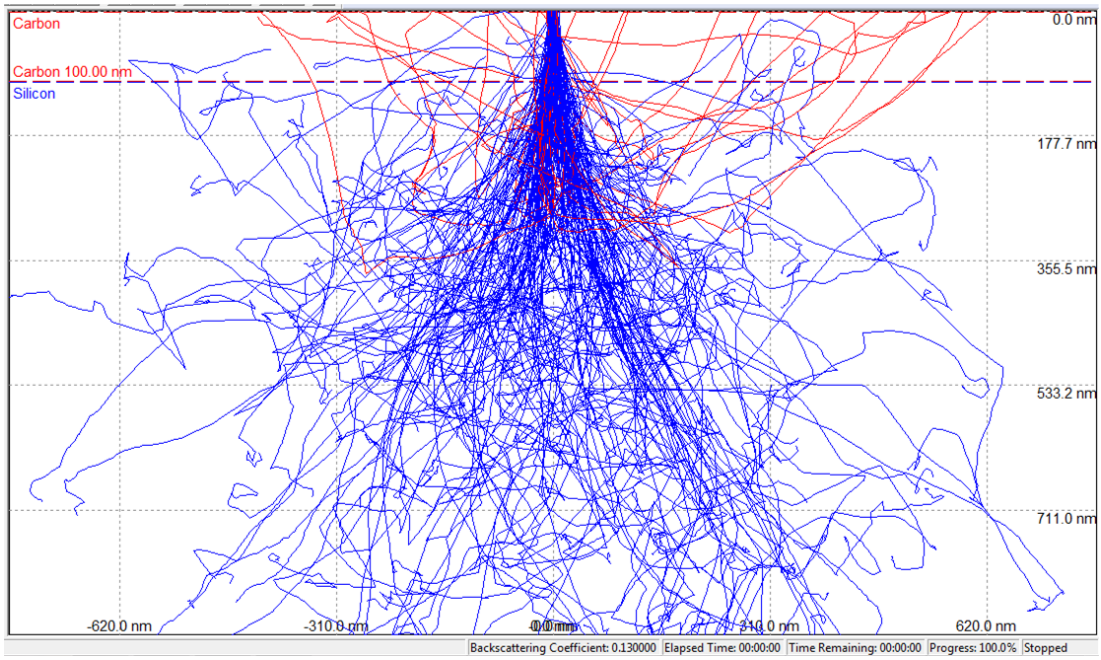

Figure 11. Electron trajectory simulation, using Monte Carlo algorithms, of an electron beam interaction with carbon (E_o =10 KeV).

These signal electrons are collected by a detector. Nowadays the most common detector is the Everhart-Thornley that works in two modes: charged positively to attract secondary electrons and charged negatively to attract backscattered electrons and reject secondary electrons with energy lower than 50eV [60]. Secondary electrons are used to

create an image of the topography of the surface of the sample thanks to the disparity in signal levels while the backscattered electrons gives information about the chemical composition as variations in levels of gray in a SEM imaged sample [61]. A phenomenon called charging of non-conductive samples and hydrocarbon contaminations should be avoided to get good images otherwise the beam will be deflected and the vacuum chamber contaminated [60].

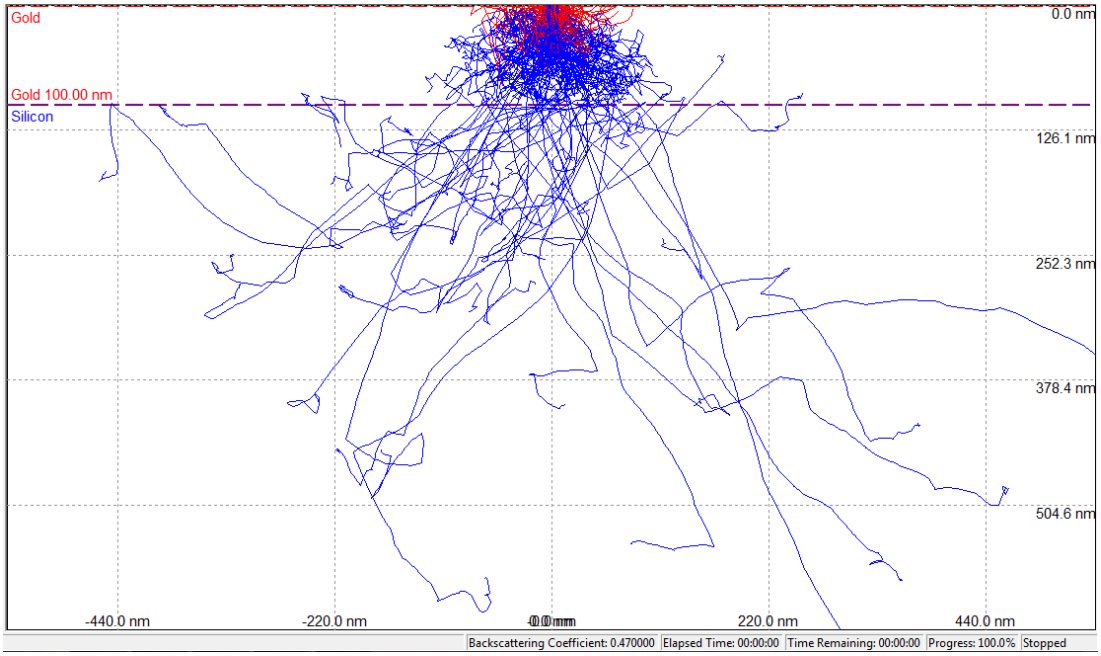

Figure 12. Electron trajectory simulation, using Monte Carlo algorithms, of an electron beam interaction with gold (E_o =10 KeV).

1.5.2 Focused Ion Beam Microscopy

Focused ion beam (FIB) is a microscopy technique suitable for metals, polymers, ceramics, composites, and fiber/powders of even difficult shapes samples for semiconductors; biological, geological, and pharmaceutical applications can also be manipulated with this tool [62]. FIB system consists of 2 columns (SEM and FIB itself)

that increase the capabilities beyond each one separately. SEM working principles were highlighted in the previous section.

FIB uses an ion beam to interact with the specimen. The interaction is similar to the electrons in SEM but because of the difference in size, the interaction between ion-atoms is higher than with electrons, which produces a decrement in ions energy and in penetration depth [63]. As result there are no backscattered electrons but sputtering of ions and neutral particles, lattice defects (vacancies and interstitial sites, dislocations and implanted ions) and secondary electrons. Furthermore, ions are heavier and can make atoms in the sample be ejected from the matrix; this fact is used to mill or sputter the specimen at nanometer scale [62].

This technique uses a source of gallium (Ga^{+}) to interact with the specimen. Gallium is a metal with low melting point which ions are heavy for sputtering and proper to create a compact and long life-time gun because of its low heating and low volatility capabilities [62]. This type of source is known as liquid metal ion source (LMIS) and is always liquid while working. The ion beam is focused with electrostatic lenses instead of electromagnetic lenses to compensate for the ions size and low velocity respect to electrons; and positioned by electrostatic quadrupole and octopole that also move it to scan over the part of interest.

During the bombardment with Ga ions many signals are generated. Those signals can be detected for several detector types to create images. Ga ions can create a channeling contrast that depends on the crystallographic orientation of the sample which means that for grains or specimens oriented in parallel to the ion beam a low contrast or low signal of SE will be detected but the opposite happens when oriented perpendicular

to the beam (Figure 13, Figure 14). In this sense, tilting of the sample allows significant changes in image contrast which is helpful in grain size analysis for example [62]. Sample size is 100x50x25mm maximum, and tilting of the specimen holder is in the range of -10° to 52°.

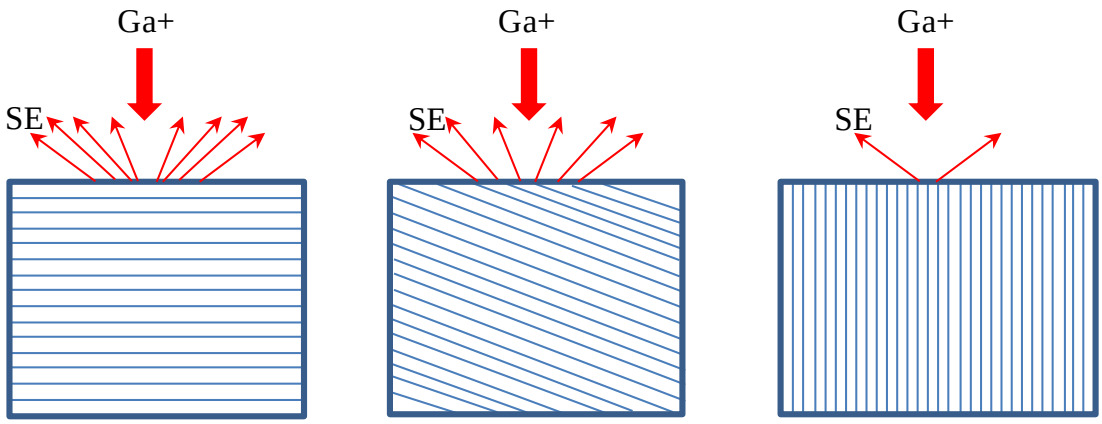

Figure 13. Schematic of the channeling contrast principle and secondary electrons generation [62].

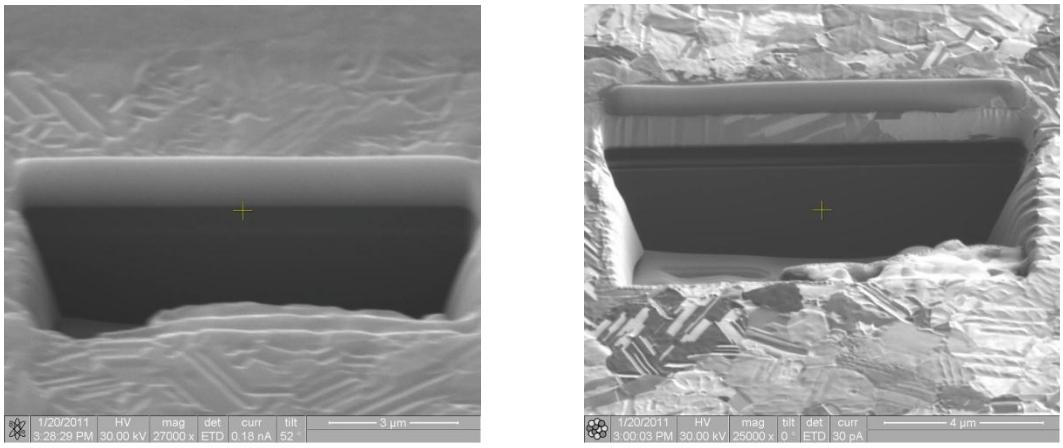
(a) (b)

Figure 14. Electron stimulated SEM (a) and Ga stimulated SEM (b).

The dual beam system consists of the 2 columns as seen below. The capabilities of this system go from milling, deposition to transmission electron microscope (TEM) sample preparation. For milling a specimen, it is able to scan a pattern as done in nano-micro fabrication and of removing atoms from the matrix to make the required opening

through even several layers of materials. This capability is also used to investigate voids and cracks within the material.

The milling process can be assisted by platinum (Pt) atoms deposited on the surface to define the edge of milling and avoid damage of the surface and subsequent layers. Deposition is done assisted by the focused ion beam when the sample is exposed to a gas rich in Pt for example; the gas is injected into the surface of interest while it is bombarded by Ga ions which make Pt atoms to deposit on an specific site of the surface [62]. Deposition can damage the surface and interfaces, to reduce this damage, the electron beam assisted deposition can be carried out with high effectiveness prior to FIB assistance. Platinum, carbon, tungsten, silicon oxide and aluminum are some of the materials appropriate for deposition. Deposition can be extended to create three-dimensional structures.

Besides all above, FIB is used to create the lamella for TEM. In this case, the specimen is milled to thin it transparent to electrons (about 100nm) in any location since the FIB can be highly positioned. This technique is very useful in view of the fact that issues such as the time spent for preparing TEM samples and the damage to the materials, have been strongly improved [63]. Recent research has given as result more capabilities for FIB/SEM dual system such as end point monitor, images from SEM image modes (SE and BSE) and Everhart-Thornley detector; images from BSE detector in A-mode, B-mode and Z-contrast; charge neutralizer, low vacuum imaging mode using a large field detector (LFD), environmental SEM mode using a gaseous secondary electron detector (GSED) and gaseous backscattered electron detector [62].

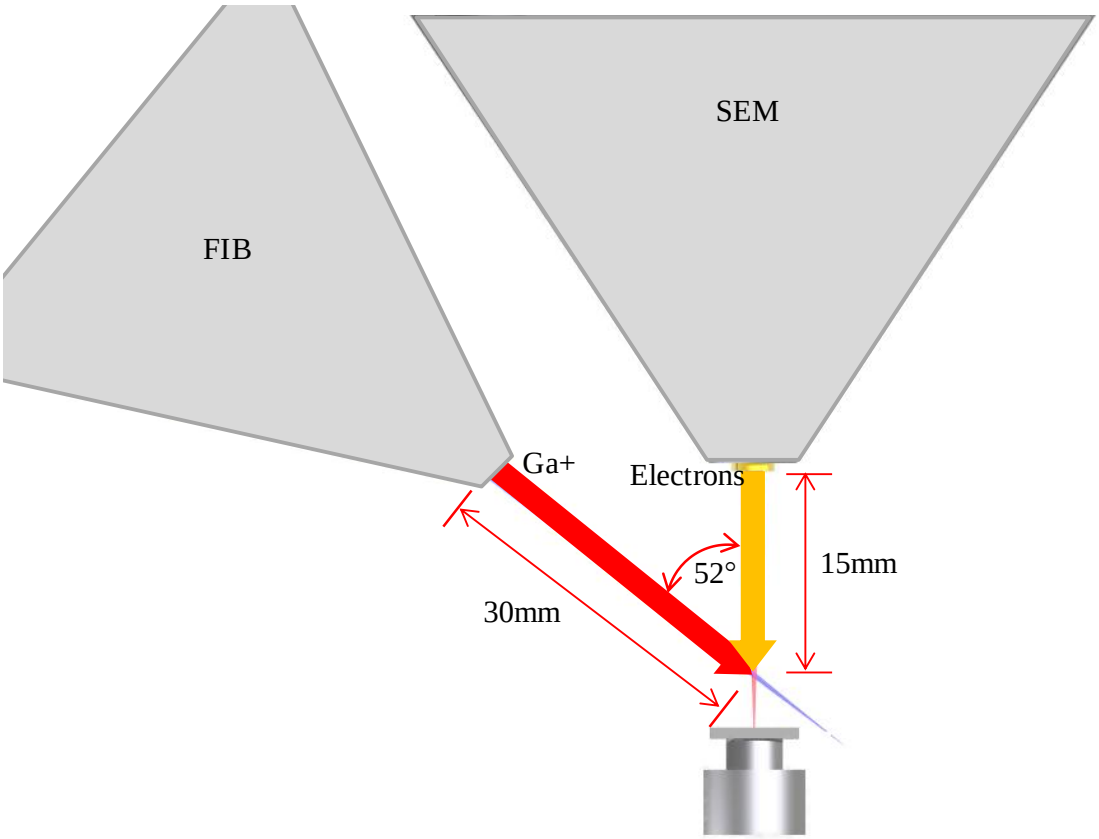

Figure 15. Schematic of a dual beam system (FIB+SEM) [62].

Chapter 2: Experimental Details

2.1 Sample Description

For this research the samples were divided into two groups. The first group was formed by two different sets of solar cells to analyze the cracks on them. The first was a set of seven commercial and completely processed monocrystalline Cz-Si solar cells pseudo-square shaped with dimensions 165mm x 165mm with a nominal thickness of 200µm (Figure 16, Figure 17) . The second set was formed by seven commercial and completely processed polycrystalline ribbon-grown Si solar cells, produced by the edge-defined film-fed growth (EFG) technique. These cells had a rectangular shape with dimensions 152mm x 76 mm and a nominal thickness of 200µm. The contacts of both sets of cells were made by screen-printing process.

The second group of samples was formed by two different sets of solar cells to analyze the influence of cracking in the efficiency and electric characteristic parameters of the cell. Both sets correspond to small pieces of solar cells with area ranging between $10cm^2$ to 70cm2 and same description as in the first group.

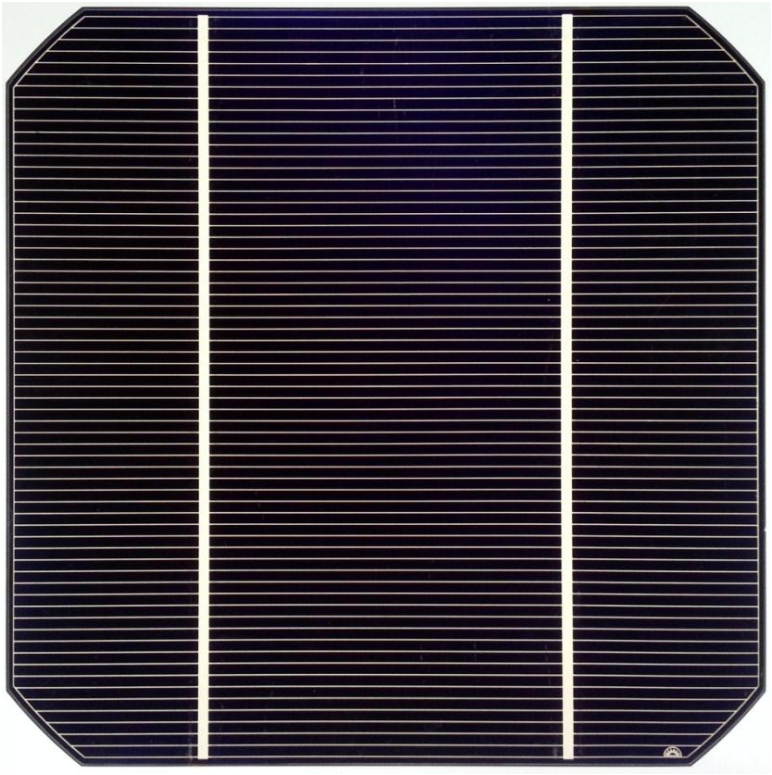

Figure 16. Czochralski Si solar cell (type 1 used).

Figure 17. Czochralski Si solar cell (type 2 used).

Figure 18. Ribbon growth (EFG) Si solar cell.

2.2 Crack Detection Techniques

2.2.1 Photoluminescence Set-up

The photoluminescence (PL) imaging tool used for this research makes use of a Spectra Diode Labs SDL 800, AlGaAs laser diode, as excitation source operating in pulse mode with emission wavelength of 800nm and a bandwidth of 10nm. The laser beam passed through lenses for focusing it on the specimen. Previous works have shown that the PL spectrum of silicon at room temperature shows defect peak band at 0.8eV [64]. Therefore the most intense luminescent band corresponding to 0.8eV was used in this project for mapping of the samples, at room temperature and with 100μm increment step in X and Y direction of a Velmex 8300 moving stage.

The emitted luminescence signal was passed through achromatic parabolic mirrors where after a SPEX-500M grating spectrometer disperse the signal emitted from the sample and separate the different wavelengths. The grating spectrometer is built in a

CCD camera. The emitted signal in the range of 1050-1550nm was then detected by a liquid nitrogen cooled germanium (Ge) detector and analyzed by a lock-in amplifier (EG&G) and sent to a computer that processes the image. The resolution of this tool is 1mm.

2.2.2 Scanning Acoustic Microscope Set-up

The scanning acoustic microscope used for the morphology investigation and finding and location of millimeter cracks is a HS1000 HiSPEEDTM by Sonix Inc which uses a high frequency ultrasonic transducer (DPR002S pulser/receiver) to emit ultrasound and detect the reflections. This transducer emits an electric pulse that is converted to mechanical energy letting the transducer to vibrate causing pulses to be sent out from the transducer. This tool is based on the pulse-echo technique with a frequency of operation up to 500MHz and a pulse repetition rate of 20KHz which avoid overlapping of echoes from one pulse with the echoes of the next pulse.

SAM was used to get information about the morphology and flaws present on the samples. To set up the tool was necessary to use deionized (DI) water bath as coupling medium since ultrasound is highly absorbed by air. The ultrasonic beam was focused to a specific depth by moving the transducer up and down (Z direction) while monitoring the output signal and its amplitude in relation to the initial time of impulse, the optimum focus was get when the amplitude of the signal got its maximum. The amplitude of the signal was increased by increasing the gain. A gate threshold (in A mode) was created to select the signal of interest, because the scan required the pulses to travel through the cell,

pulses reflected from the back surface were chosen to analyze what was happening in the bulk (within the material).

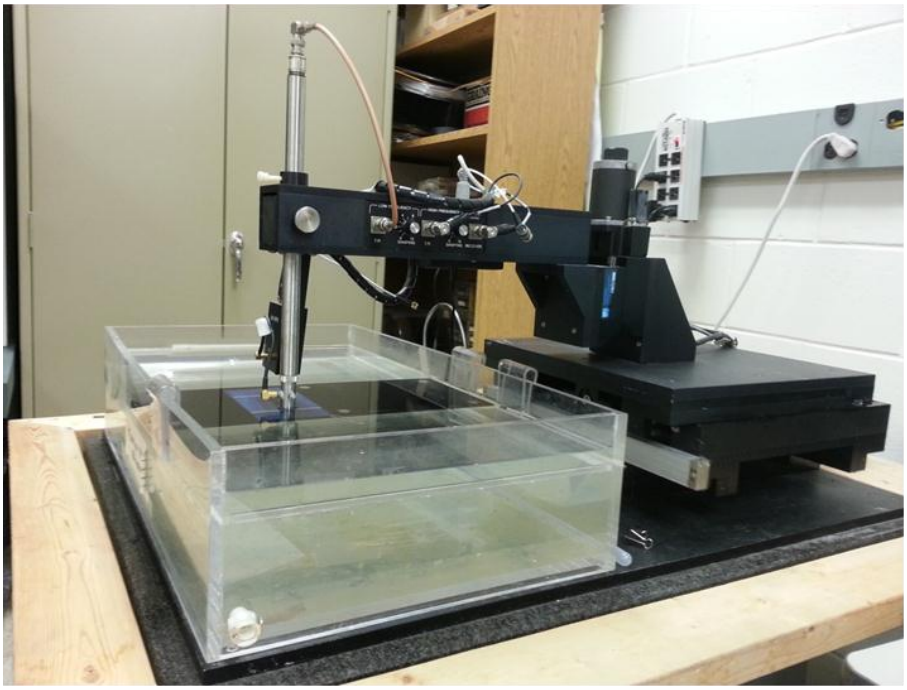

Figure 19. Scanning acoustic microscope HS1000 HiSPEEDTM.

A required threshold for the front surface reflection was also set as ‘front surface follower’ by moving the transducer in X and Y direction along the sample and positioning the follower to keep the signal in the appropriate range (within the sample). Reflections from each interface hit by the ultrasonic beam were used by the SAM to create the image. The system was set up to scan the sample with a step size of 100um and 50um for high resolution data acquisition, speed of 100mm/s and acceleration of 1000mm/s^2.

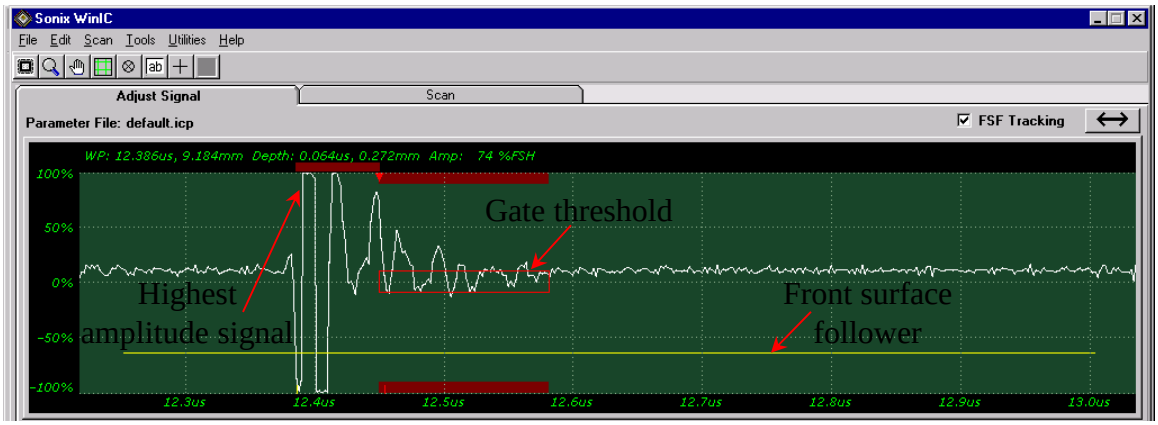

Figure 20. Typical signal in A-mode showing the front surface follower and gate thresholds.

2.3 Crack Shape and Propagation Depth: Investigation Methods

2.3.1 Electron Stimulated SEM, Ion Stimulated SEM and FIB

The crack analysis was made using a FEI Quanta 200 3D dual system that incorporates SEM and FIB in the same tool taking advantage of its separate capabilities. The electrons stimulated SEM was used for positioning on the sample site of interest. An electron beam of 30KV was used for imaging and an Everhart-Thornley detector (ETD) in SE mode, which detect secondary electrons produced by the sample from the interaction with the electrons beam to image the sample's topography.

For ion bombardment and cross sectioning the sample was tilted 52° to allow for the ion bean to strike the surface of interest perpendicularly. When in that location, ion stimulated SEM with an ion beam of 30KV perpendicular to the sample was used to ensure that the location is the appropriate. A platinum layer of 1µm thick was deposited in the surface for protection before milling. The platinum source is trimethyl methylcyclopentadienyl platinum ($C_5H_4CH_3Pt(CH_3)_3$) contained in a gas injection system

(GIS) needle that warms it up at prior to deposition. This platinum source is a low-melting point solid, turning to liquid at 30℃.

Figure 21. FEI Quanta 200 3D dual system.

The cross section was done with a Ga+ beam of 30KV. The regular milling removed atoms from the surface and deeper to expose the material. A posterior milling is done close to the deposited Pt to smooth the cross sectioned surface and reveal clearly features within the material.

2.4 Characterization of Solar Cells

The cells' characterization was done by measuring the characteristics voltage and current at different loads (resistance values). A plot of the voltage and current obtained

were used to get the electrical performance parameters Voc and Isc and maximum voltage and current to determine the conversion efficiency and full fill factor.

The current was measured using a Keithley 2400 High Current SourceMeter®, this model has a maximum power of 22W and resolution capabilities enough to measure I-V curves of any single junction cells and in dark conditions. The measured current can range from 10pA to 1.055A. The voltage was measured using a Craftsman multimeter. The load was provided by a Phipps and Bird, Inc. resistance substitution model 236A. The sunlight source was simulated using a GE® 100W incandescent bulb with 1230 lumens of illumination. The light intensity was measured at different distances with a Li-Cor® pyranometer model PY 64059. The distance between the lamp/bulb and the pyranometer was changed to obtain the curve of light intensity versus distance for the incandescent bulb given in Figure 22. The incident power in W/m^2 is calculated by multiplying the intensity in mV by 74.5 (as specified in the pyranometer). For the experiments the minimum height reached by the lamp used was 3cm for which the incident power is about $871.65W/m^2$.

The set-up shown in Figure 23 corresponds to the circuit shown in Figure 24 and was used for output current and voltage measurements. The positive terminal of the cell is the back surface contact and the negative terminal is any of the front surface contact.

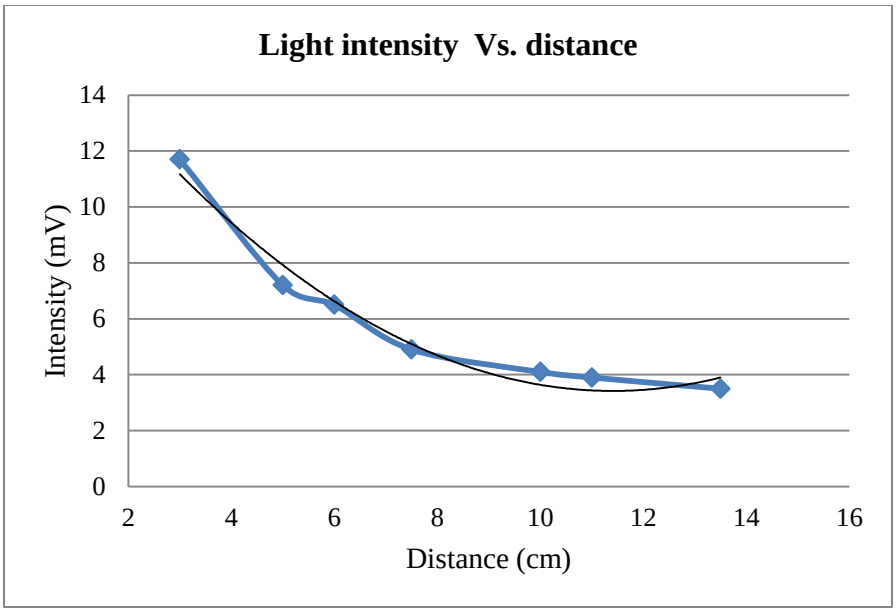

Figure 22. Light intensity as function of the distance between the incandescent bulb and the pyranometer.

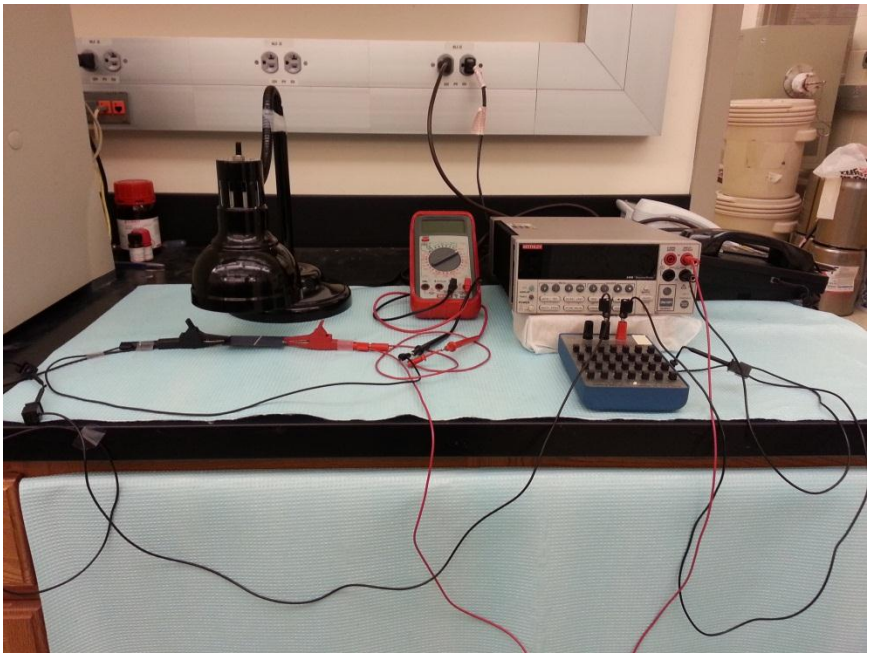
Figure 23. Set-up for output voltage and current measurements.

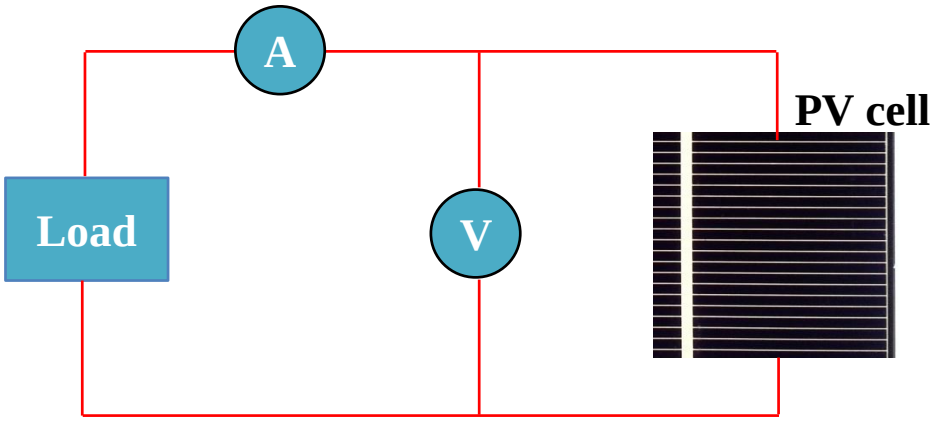

Figure 24. Circuit for output voltage and current measurements.

Chapter 3: Results

3.1 Solar Cell Layers Investigation

The thickness of the solar cell layers for single and polycrystalline silicon were measured and compared. For single silicon cells the thickness of the silicon layer was about 150µm of which around 5µm is n-type silicon. The back contact is made of aluminum paste with a thickness of 40µm, the surface contacts are also made of aluminum paste. In the process of getting the sample for FBI/SEM dual system, the silicon layer was broken unintentionally in the longitudinal direction as seen in Figure 25 and Figure 26.

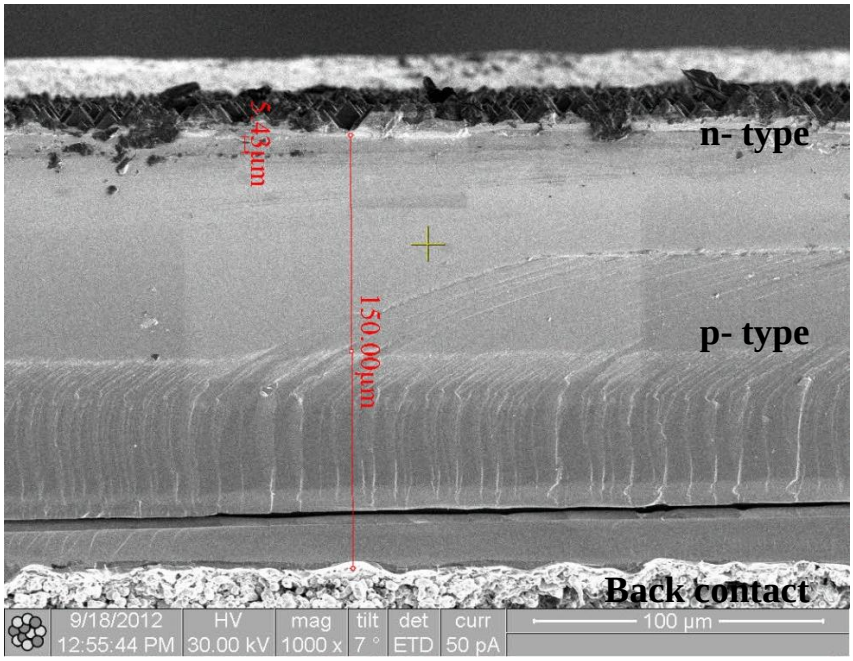

Figure 25. Ions stimulated SEM of an edge of a single crystal solar cell showing the thickness of the n- and p- type layers.

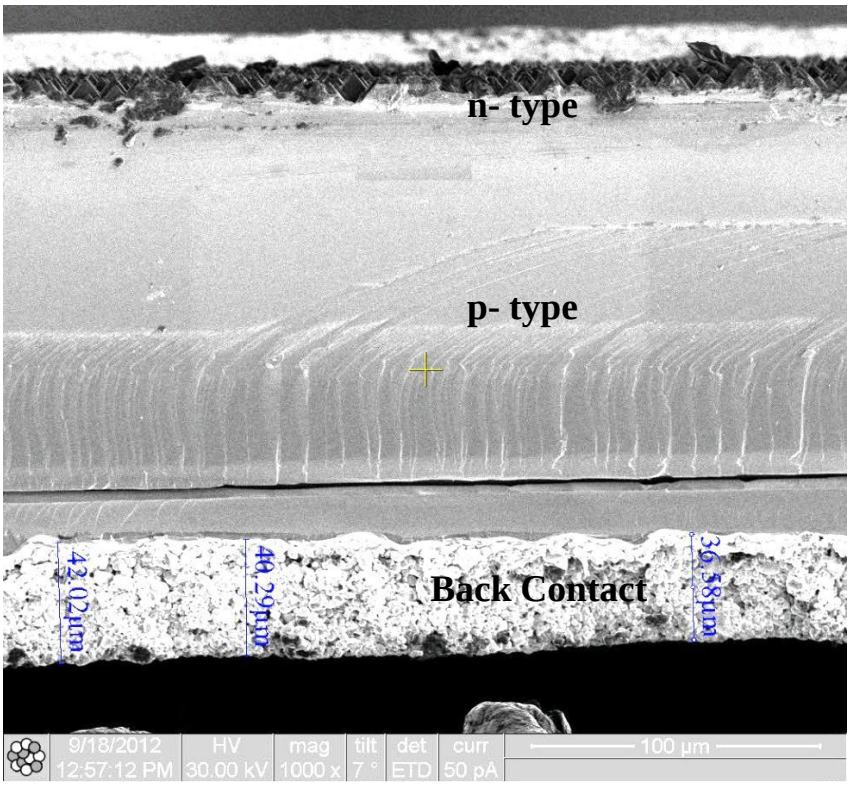

Figure 26. Ions stimulated SEM of an edge of a single crystal solar cell showing the thickness of the back contact.

Back contact layer is showed in detail in Figure 27, Figure 28 and Figure 29. The bulk particulate and porous microstructure of the aluminum is clearly seen. Figure 28 shows the highly p-doped silicon layer (back surface field-BSF) above the eutectic layer of the aluminum bulk.

The same procedure was done for polycrystalline silicon solar cells with similar results. Figure 30 and Figure 31 show electrons stimulated SEM images of a polycrystalline cell. The thickness of the p-doped silicon was about 143µm and for the n-type layer was around 4µm is n-type silicon. The back contact is made of aluminum paste with a thickness of 40µm, the front surface contacts are also made of aluminum paste.

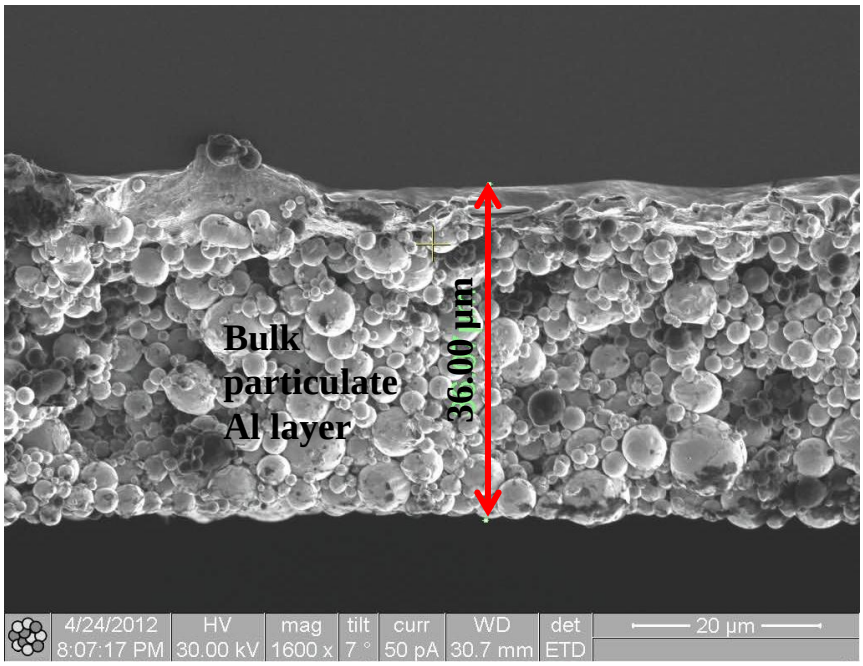

Figure 27. Ions stimulated SEM showing back contact layer.

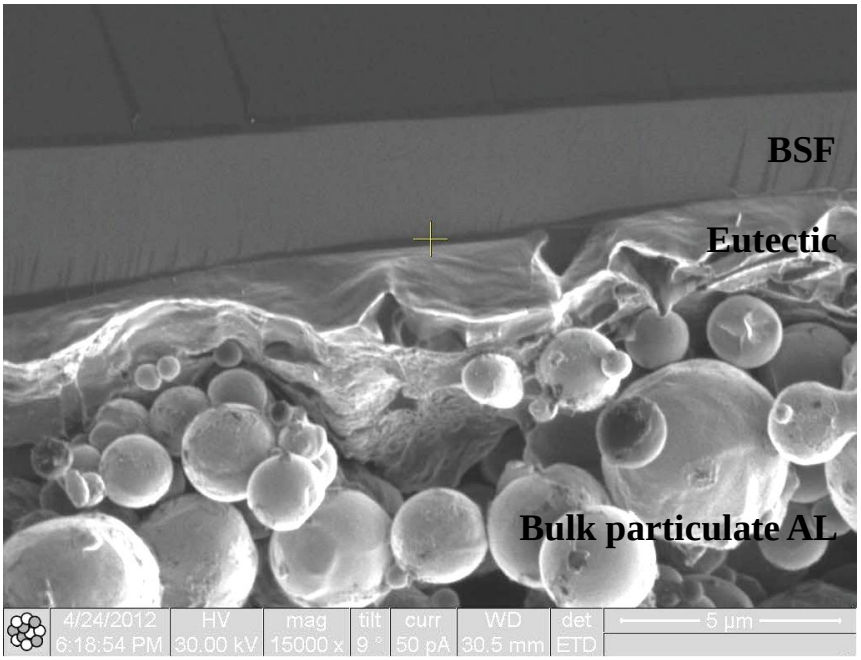

Figure 28. Ions stimulated SEM showing the BSF, eutectic and back contact layer.

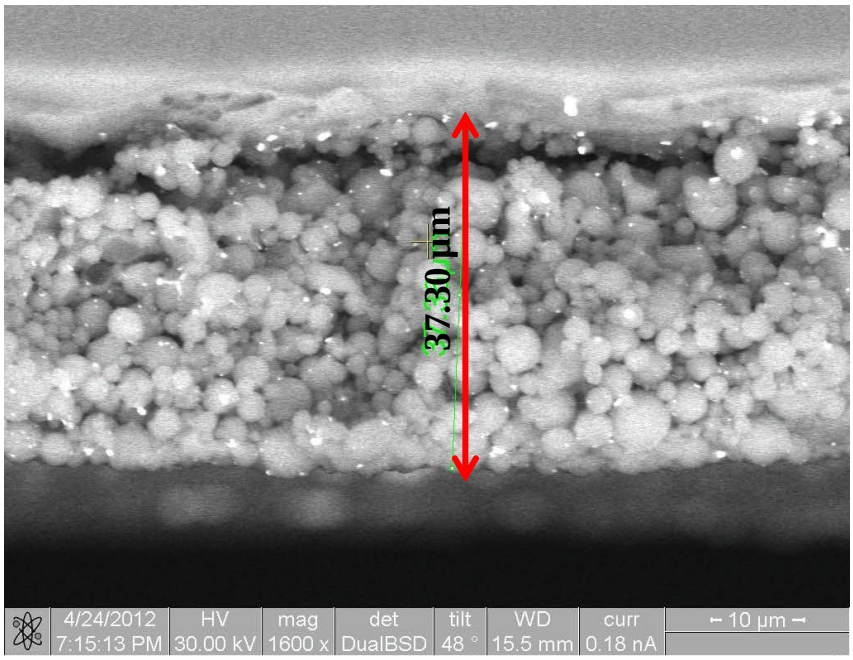

Figure 29. Electrons stimulated SEM of the back contact layer.

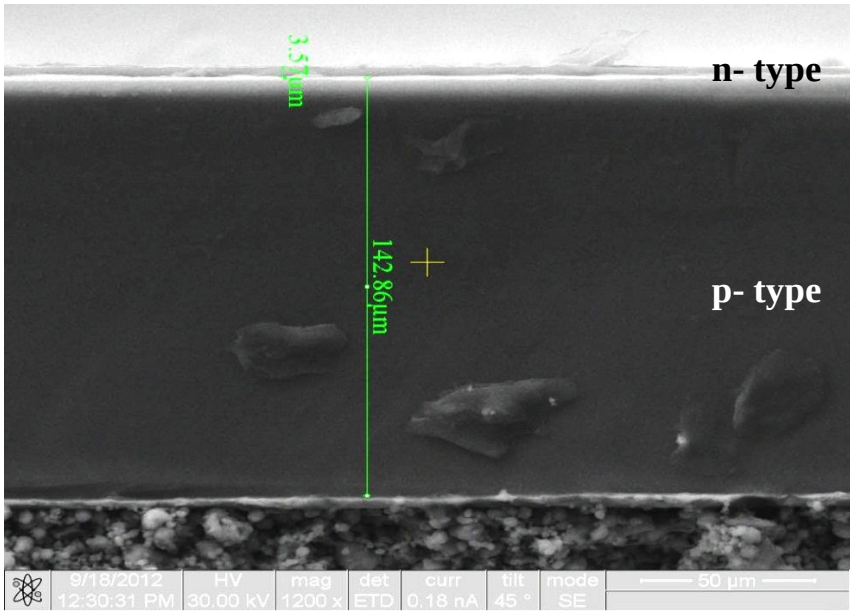

Figure 30. Electrons stimulated SEM of an edge of a polycrystalline solar cell showing the thickness of the n- and p- type layers.

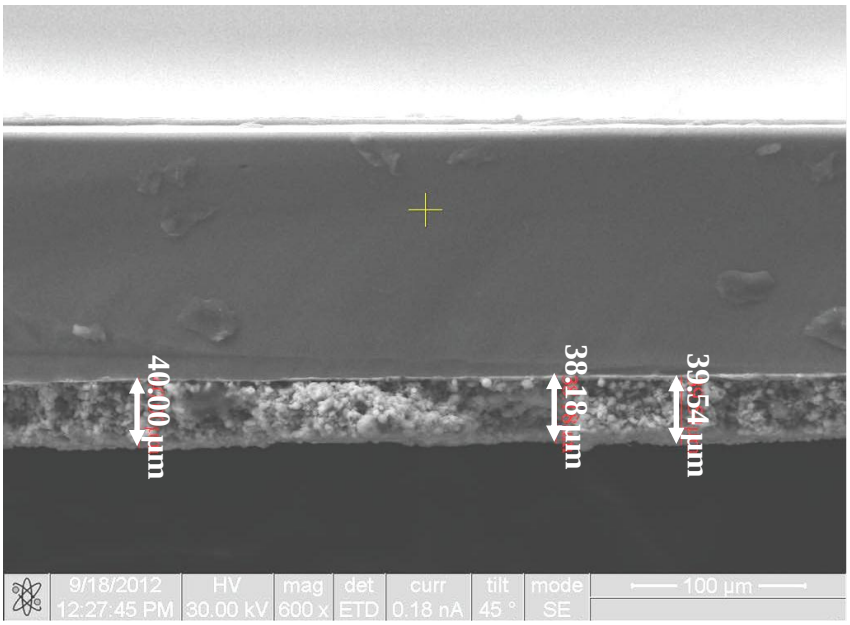

Figure 31. Electrons stimulated SEM of an edge of a polycrystalline solar cell showing the thickness of the back contact.

3.2 PL and SAM Comparison

To establish the crack detection method to use in this research project there were compared two different imaging techniques suitable for solar cells such as PL and SAM. Single silicon solar cells with and without cracks were analyzed using both methods. First sample showed multiple features in PL (Figure 32-a); but in SAM no cracks or features were identified (Figure 32-b). The second sample showed the same behavior as before (Figure 33).

In the subsequent samples similar results were obtained. As may be observed in Figure 34(a) there is a missed crack under the contact, a corner crack longer than in (b) and a non-crack feature which is framed in Figure 34(a)-Loc 2. In Figure 35 (a) a long crack seems to be located in between the contact,s and in (b) the same crack but shorter in length was observed.

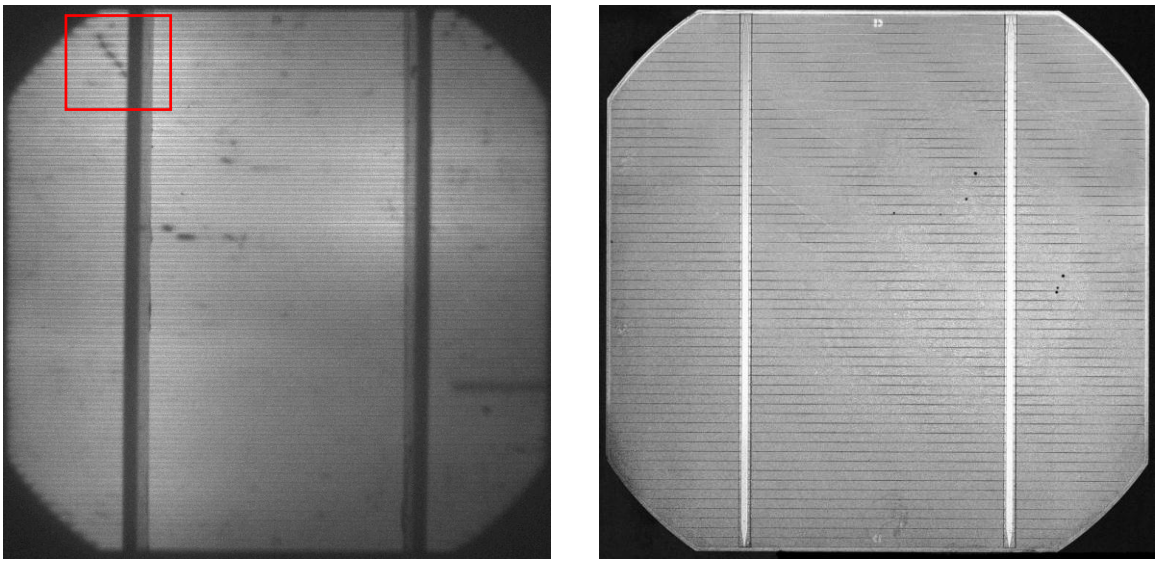

(a) (b)

Figure 32. Sample 1 features showed with (a) PL and (b) SAM.

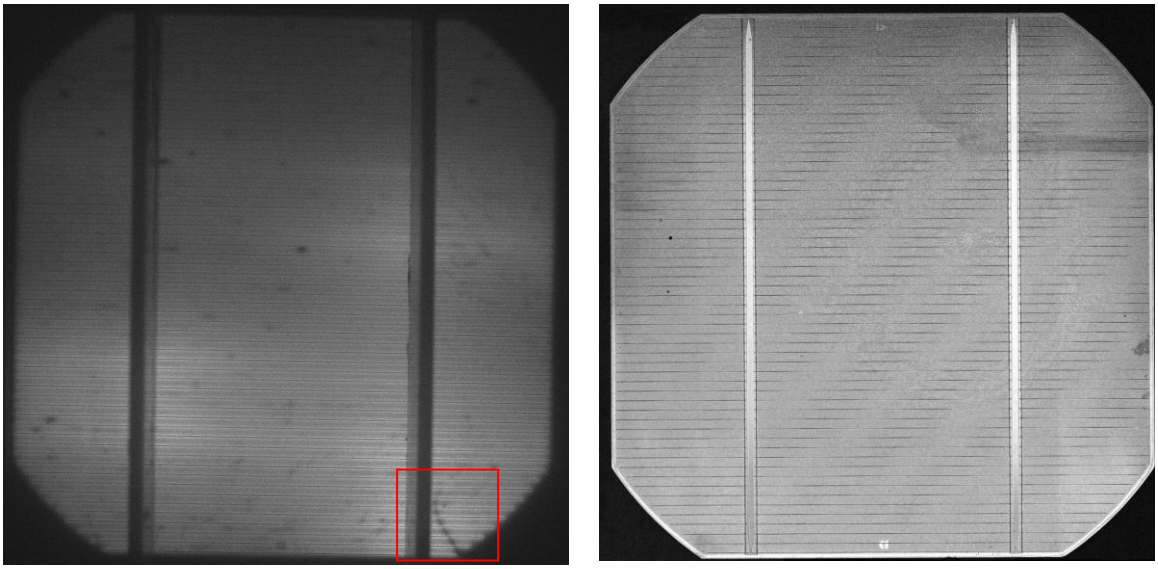

(a) (b)

Figure 33. Sample 2 features showed with (a) PL and (b) SAM.

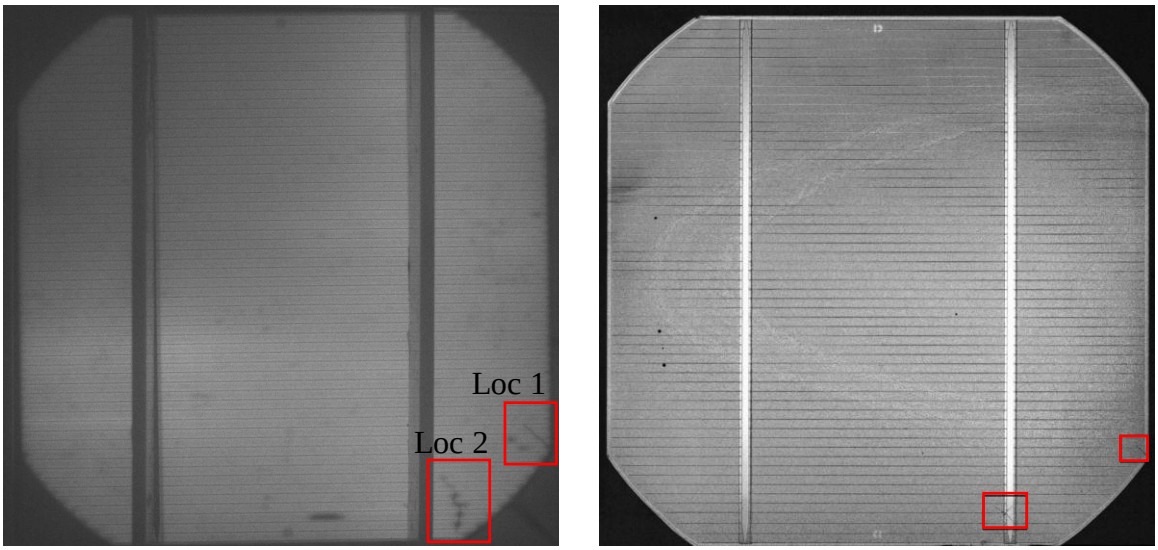

(a) (b)

Figure 34. Sample 3 features showed with (a) PL and (b) SAM.

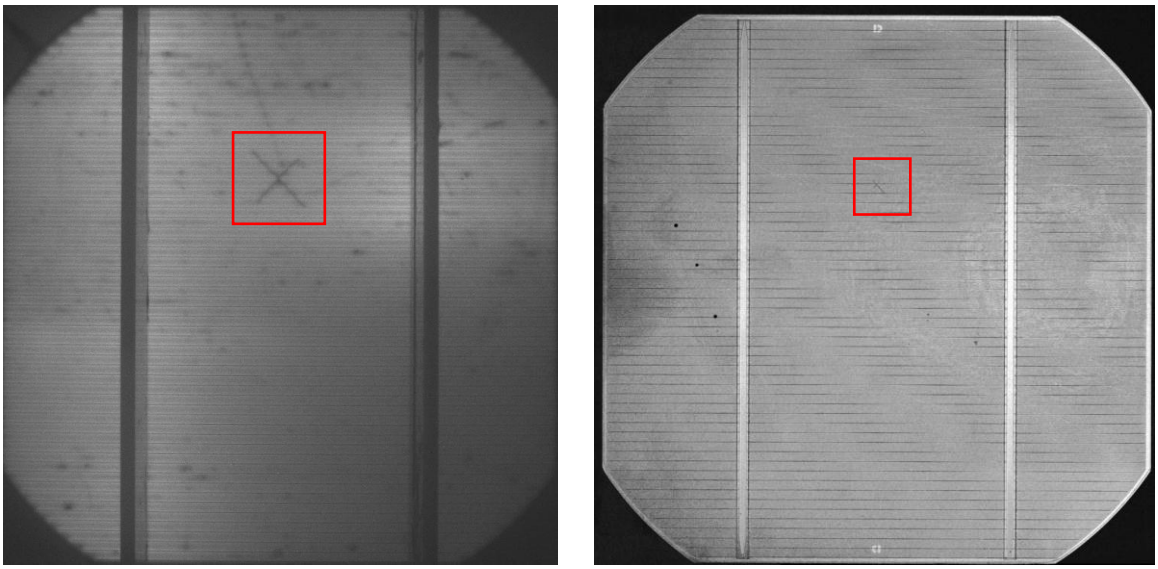

(a) (b)

Figure 35. Sample 4 features showed with (a) PL and (b) SAM.

3.3 Crack Analysis: SEM/FIB Cross-Section

After the suspected cracks were located, an investigation using FIB cross-section was performed to ensure the location, and existence of the crack. Sample 3 was used in two different locations (Loc 1 and 2), highlighted in Figure 34. The monocrystalline

silicon solar cells used in this research have on its surface an antireflection coating that prevents the SEM for clear visualization of the crack in the surface of the cell as noticed in Figure 36.

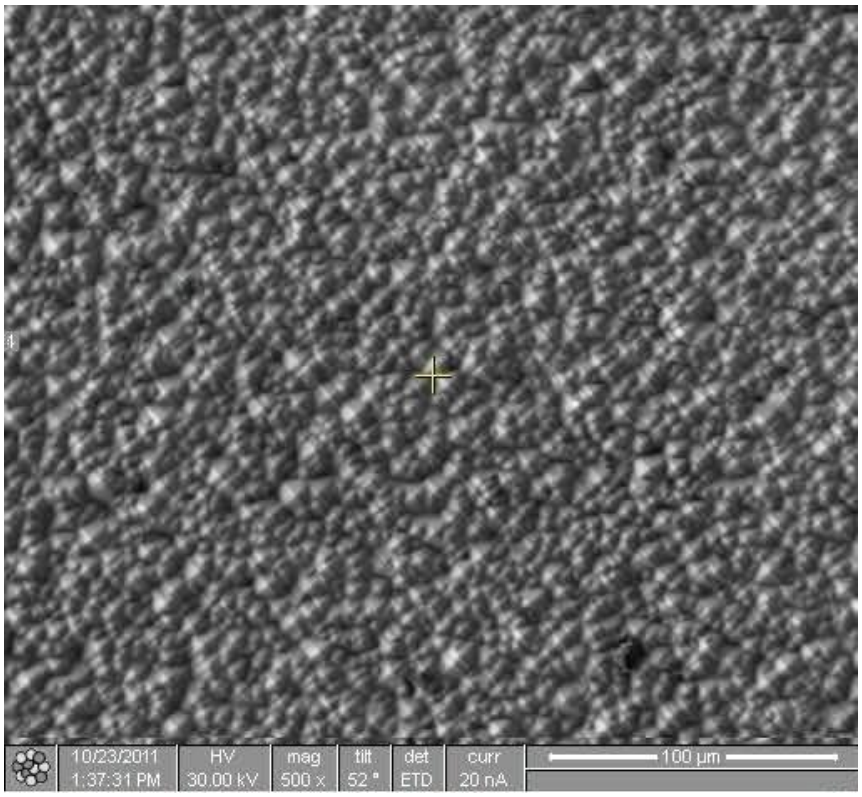

Figure 36. Sample 3-location 1 seen from the surface with ions stimulated SEM showing no dominate cracks visible.

FIB cross-section was carried out in the location specified by SAM. The pictures below confirm the existence and proper location of the crack. The propagated crack was slightly seen using electron stimulated SEM as showed in Figure 37. Figure 38 shows clearly the crack using ions stimulated SEM; change in phase is also clearly seen. The depth of the crack is more than 15µm (Figure 38); the crack penetrates through 3.46µm of n-type silicon (Figure 25) and propagates into p-type silicon. This crack is visible in all depth of view with a direction of propagation inside the silicon of about 45º.

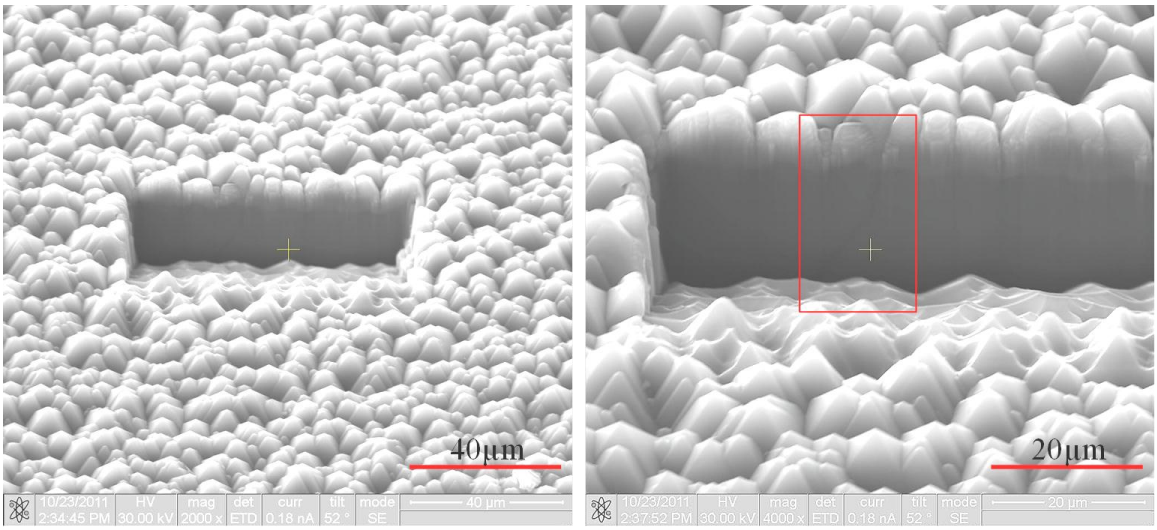

(a) (b)

Figure 37. FIB cross-section in the suspected crack in sample 3-location 1 seen with electron stimulated SEM at different magnifications.

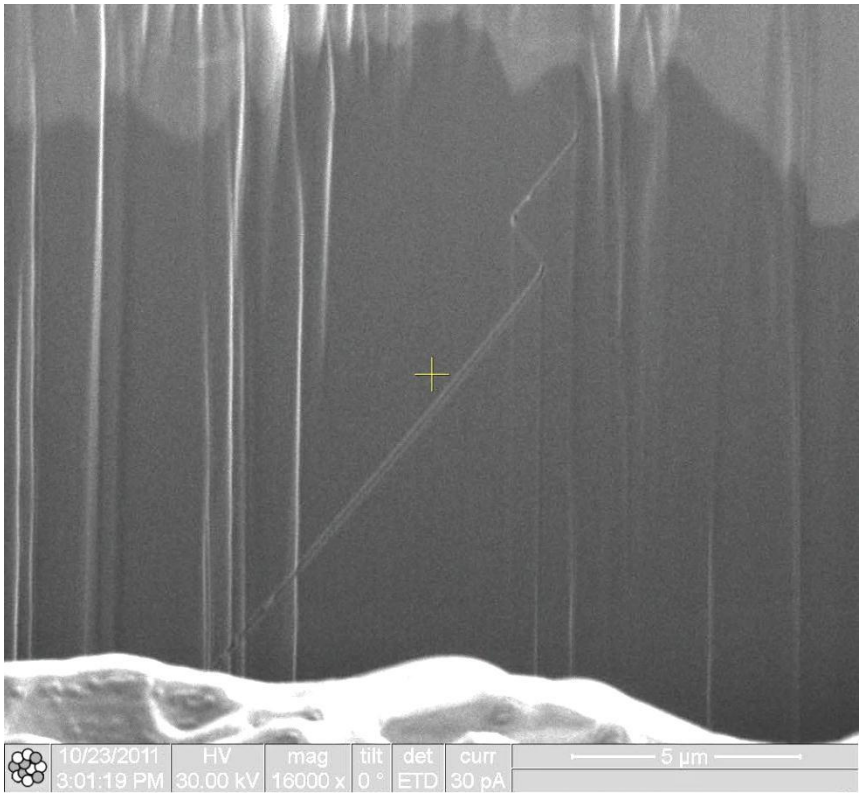

Figure 38. FIB cross-section in sample 3-location 1 seen with ions stimulated SEM.

Images from location 2 (Figure 39) showed no crack on the cross-section when seen with ions and electrons stimulated SEM. This allows to conclude that cracks can be misled using PL, and SAM could be used as a more reliable method for crack detection.

SAM was used to find location of cracks in polycrystalline samples (frame in Figure 40). FIB/SEM was carry out to confirm the crack found with SAM in polycrystalline silicon solar cells, but in this case the crack is visible with ions stimulated SEM even on the surface of the cell (Figure 41). Roughness of this surface is less than in single crystal cells where the conic structure of the antireflective coating makes cracks non-visible. After FIB cross section the crack is totally confirmed (Figure 42).

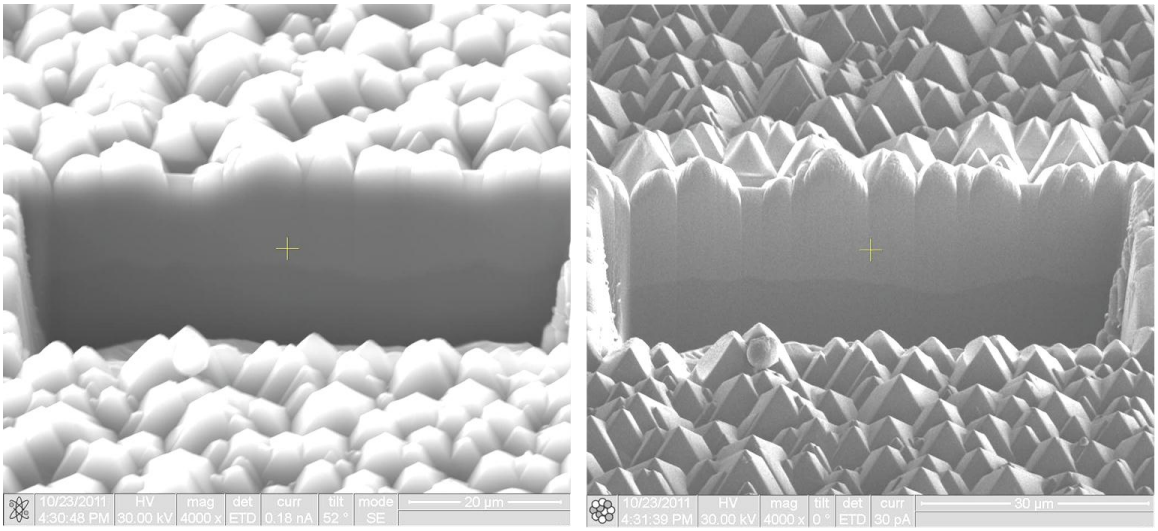

(a) (b)

Figure 39. FIB cross-section of the suspected crack in location 2 seen with (a) electron stimulated and (b) ions stimulated SEM.

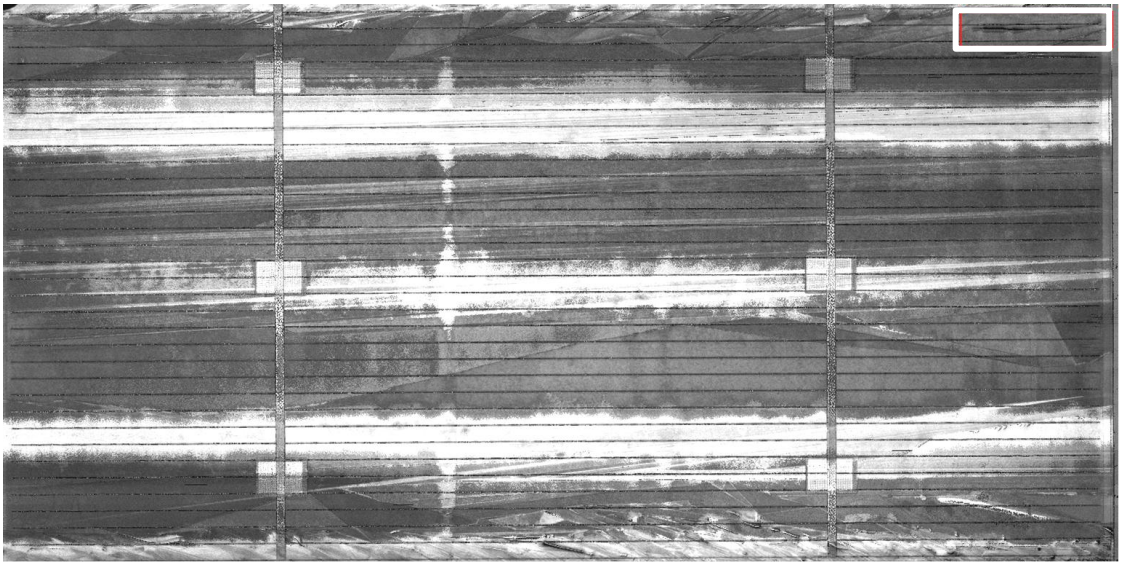

Figure 40. Crack in a polycrystalline silicon cell seen by SAM.

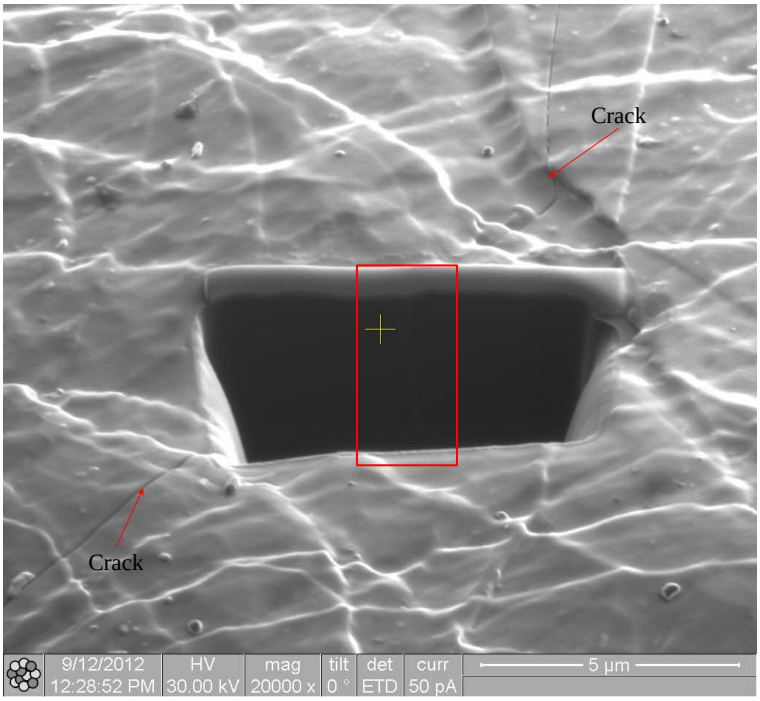

Figure 41. Crack in a polycrystalline silicon cell seen from the surface with ions stimulated SEM.

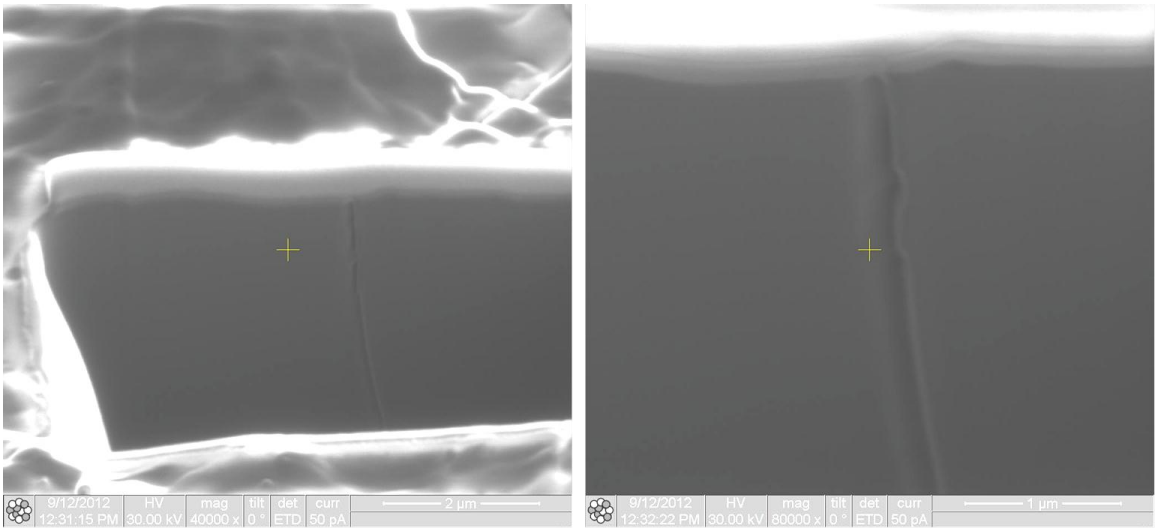

(a) (b)

Figure 42. FIB cross-section of a polycrystalline silicon solar cell in the crack location seen with ions stimulated SEM.

3.4 Analysis of Electric Characteristics of Solar Cells Before and After Cracking

Characteristic output curves were obtained for 5 monocrystalline silicon solar cell samples and 5 polycrystalline silicon solar cell samples before and after cracking. Cracks were induced by letting fall a sharp tip on the front surface of the cell. The highest incident power from the incandescent bulb was reached at 3cm (see section 2.3.1) with 871.65W/m^2.

The following figures show SAM images of monocrystalline samples 1 to 5 before and after cracking. As may be seen in Figure 46 sample 4 was previously cracked but still cracks were induced to compare the drop in efficiency after and before. Figure 48 to Figure 52 show the response of single crystal cell pieces to the input power mentioned above. Each point of the curve corresponds to the response of the cell to a change in load. The resistance values used: 0Ω (short circuit), 1Ω, 2Ω, 3Ω, 4Ω, 5Ω, 10Ω, 20Ω, 50Ω, 100Ω, 200Ω, and open circuit.

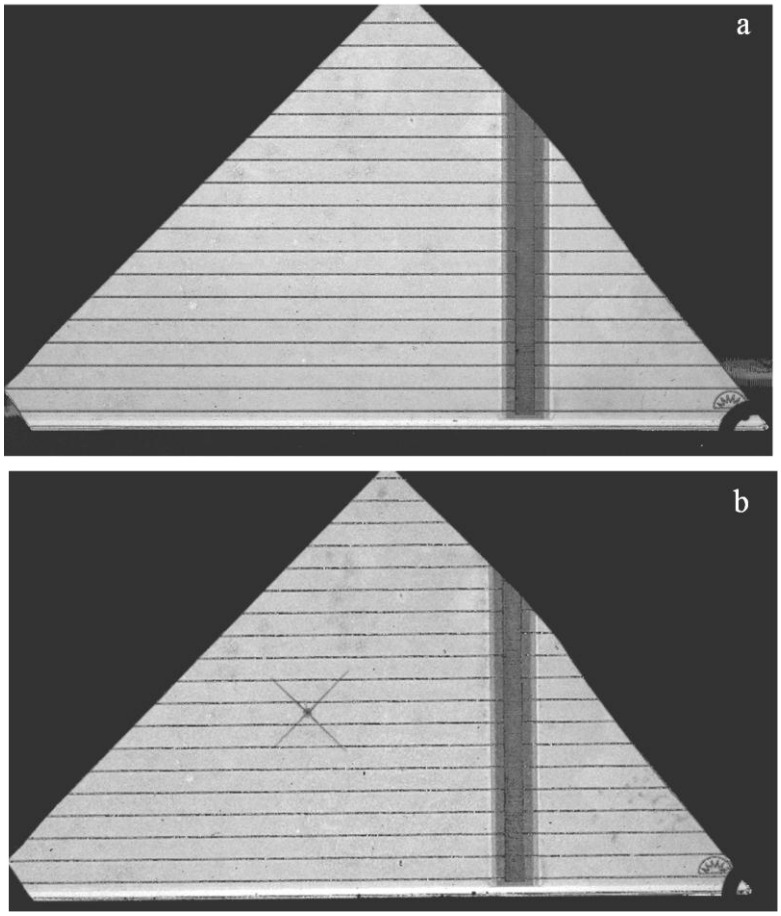

Figure 43. SAM of monocrystalline sample 1 (a) before and (b) after cracking.

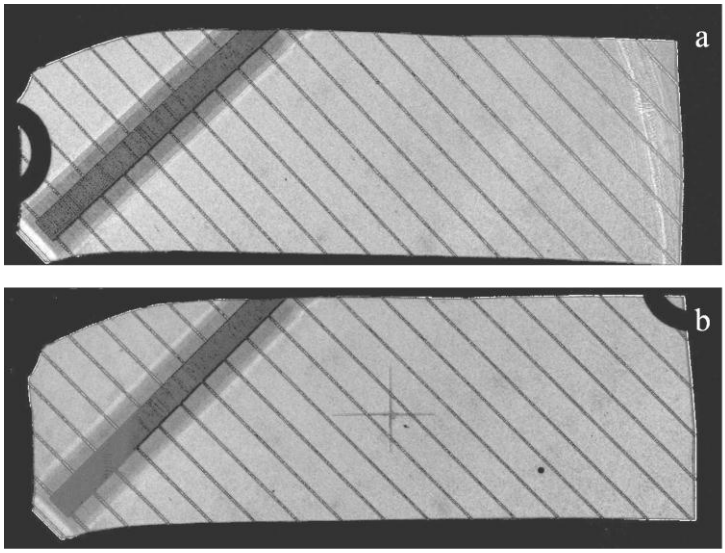

Figure 44. SAM of monocrystalline sample 2 (a) before and (b) after cracking.

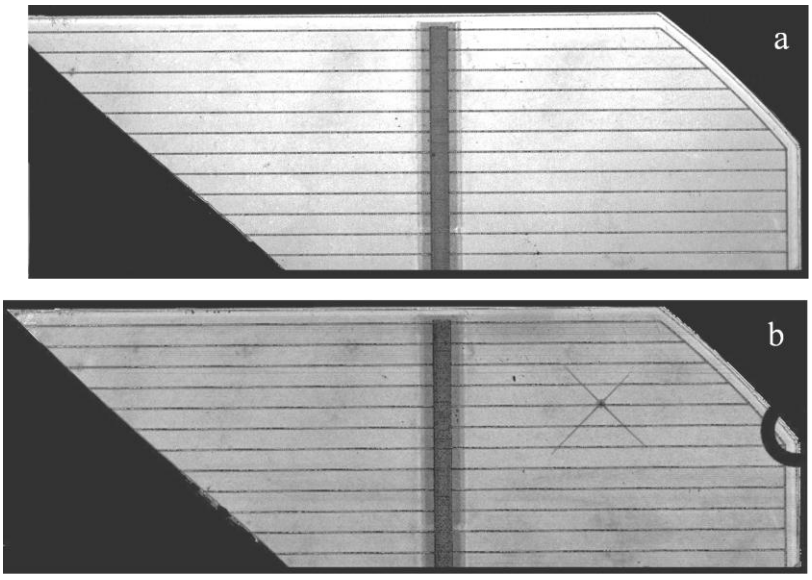

Figure 45. SAM of monocrystalline sample 3 (a) before and (b) after cracking.

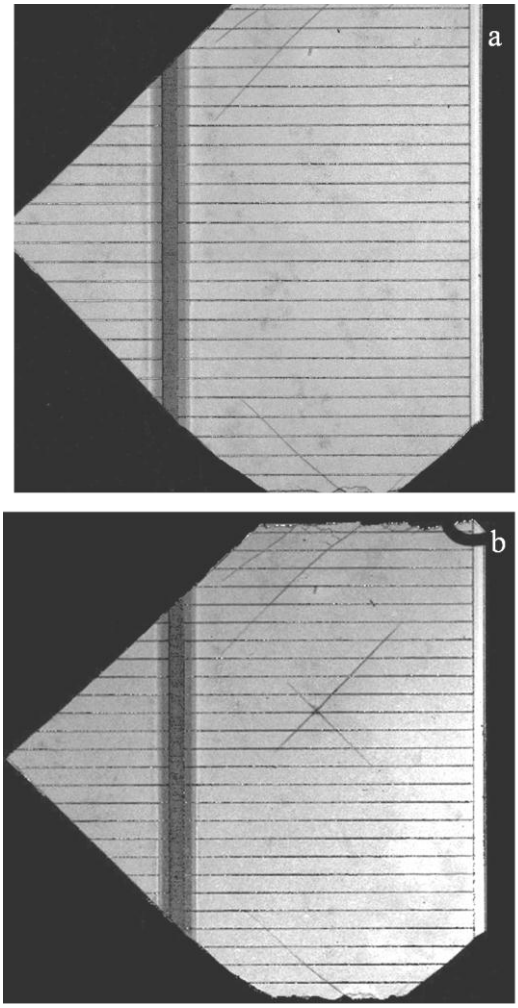

Figure 46. SAM of monocrystalline sample 4 (a) before and (b) after cracking.

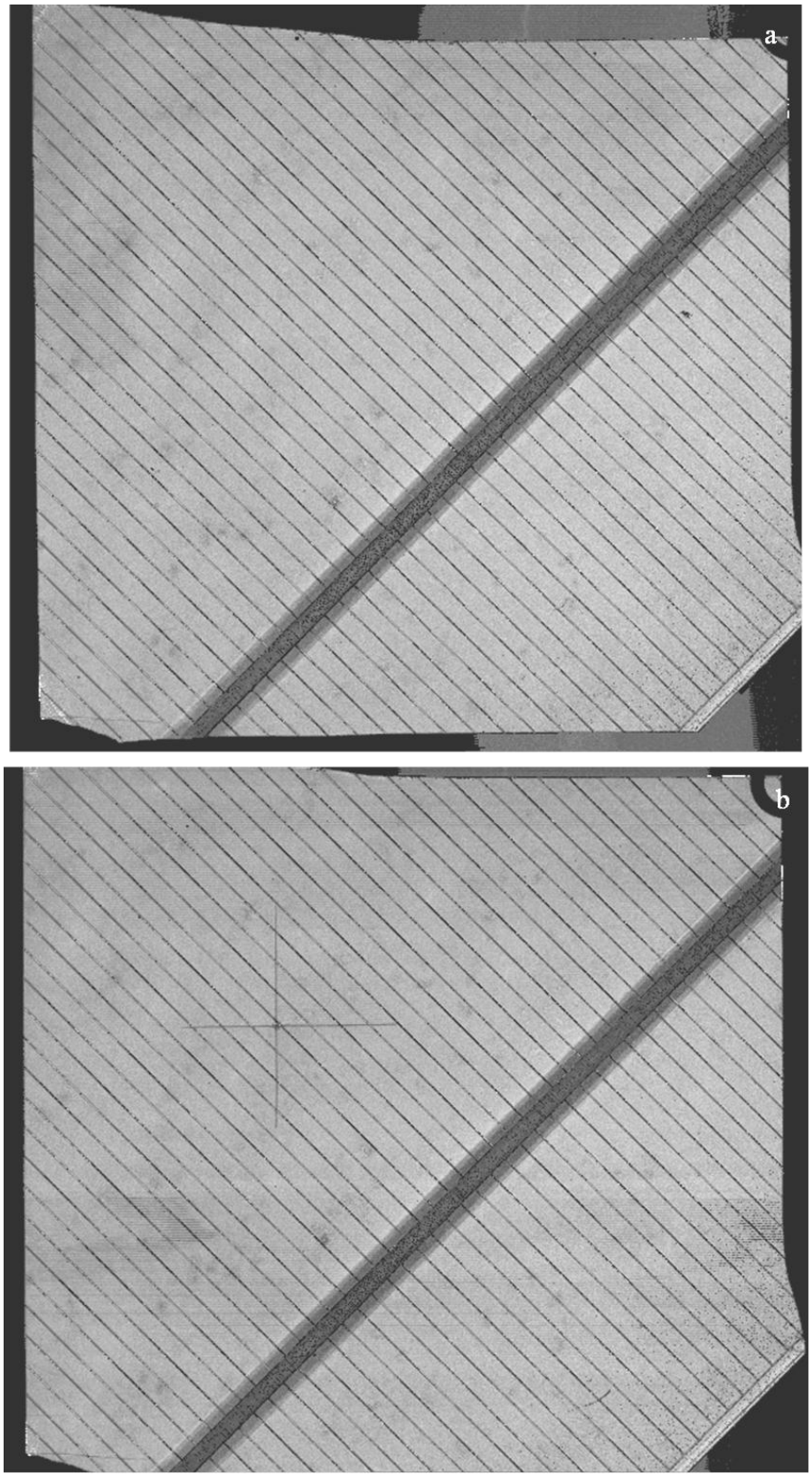

Figure 47. SAM of monocrystalline sample 5 (a) before and (b) after cracking.

For each sample there were taken at least three measurements per each load (resistance) value. The following figures show the characteristic output response of the monocrystalline samples before and after cracking for monocrystalline samples 1-5.

A clear difference in the characteristic parameters can be noticed while the shape of the curve is kept. The shape of the curve does not match the real curve, this could be caused by the series and shunt resistances increment during the initial and subsequent breakage of the cells. Same behavior is shown in the other samples.

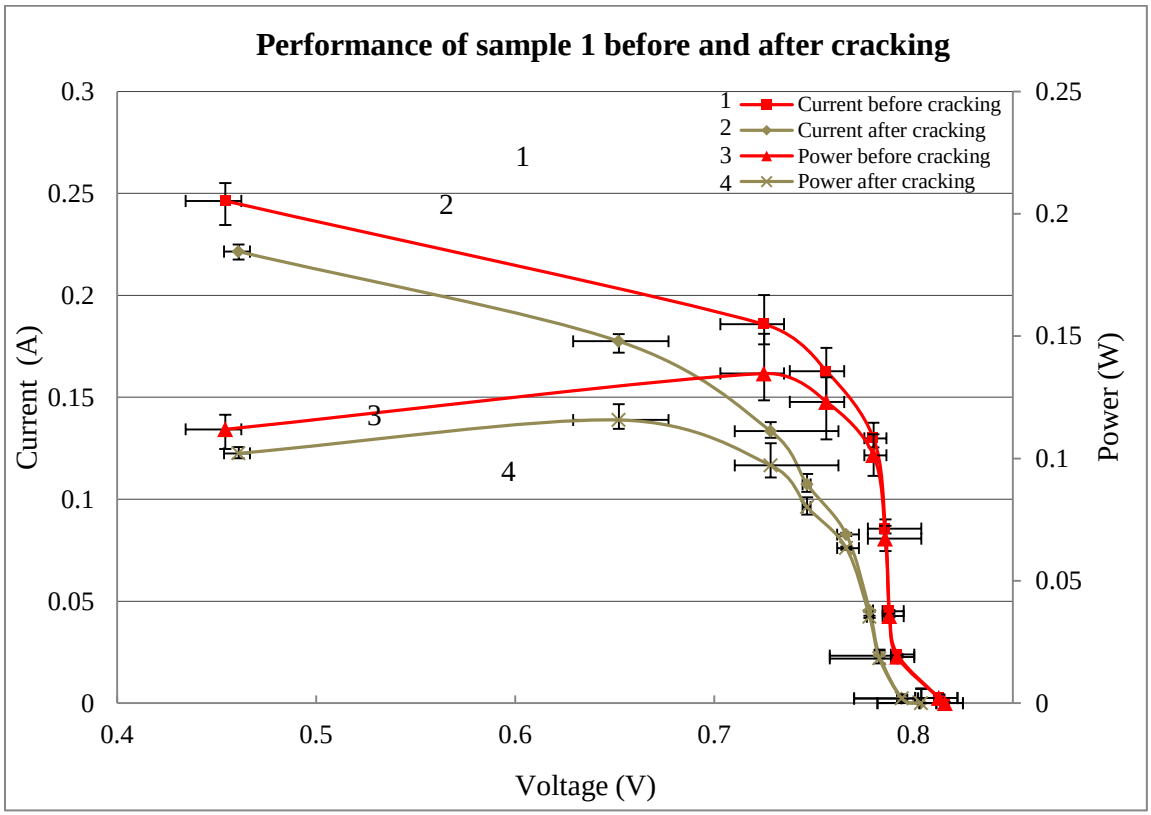

Figure 48. I-V curve of monocrystalline sample 1 before and after cracking.

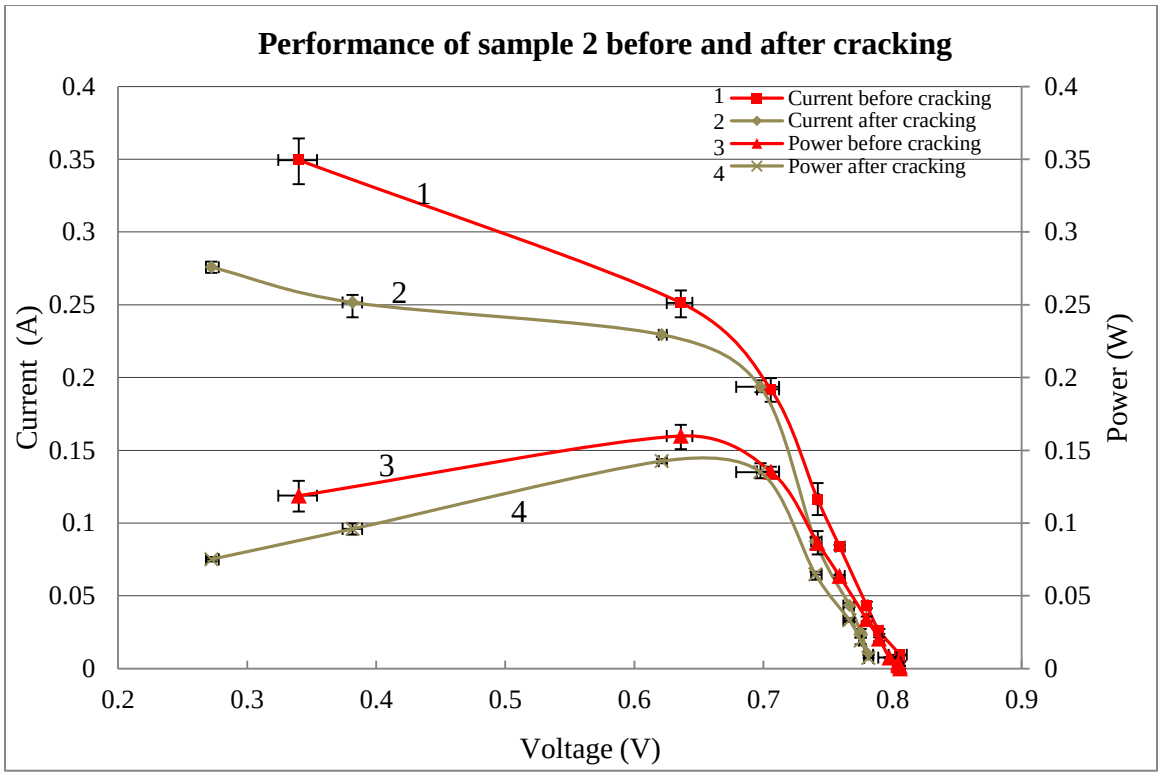

Figure 49. I-V curve of monocrystalline sample 2 before and after cracking.

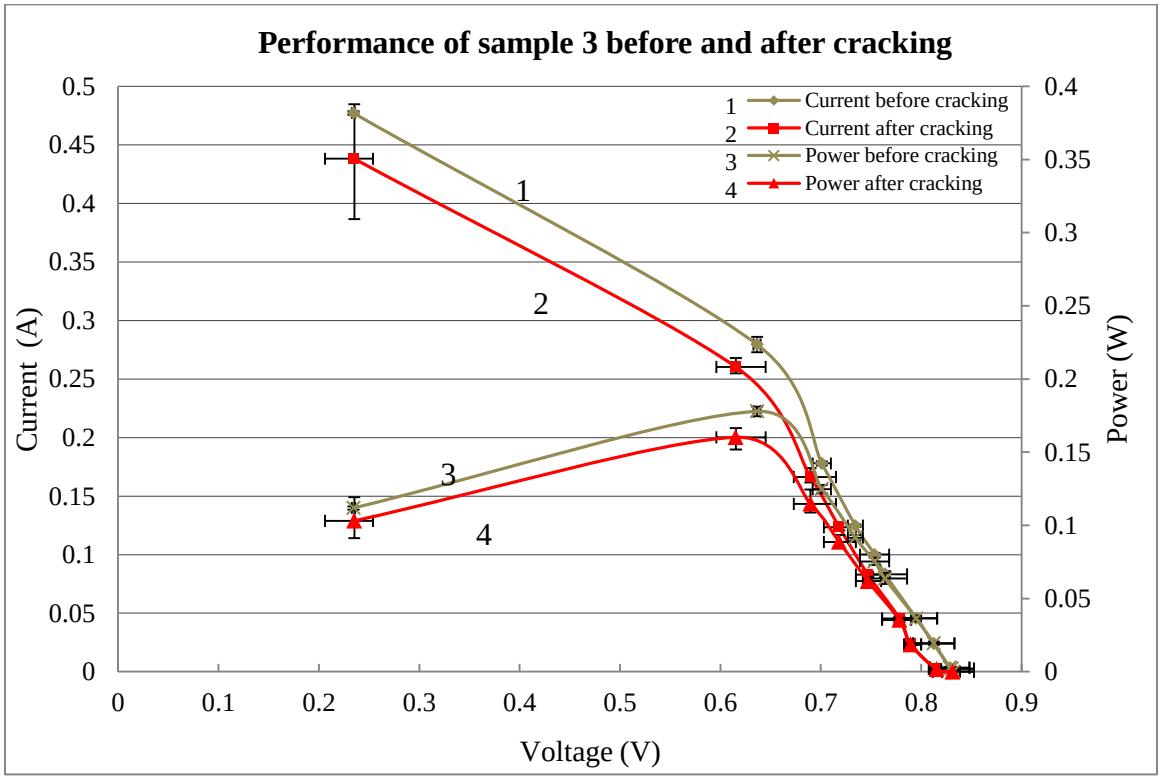

Figure 50. I-V curve of monocrystalline sample 3 before and after cracking.

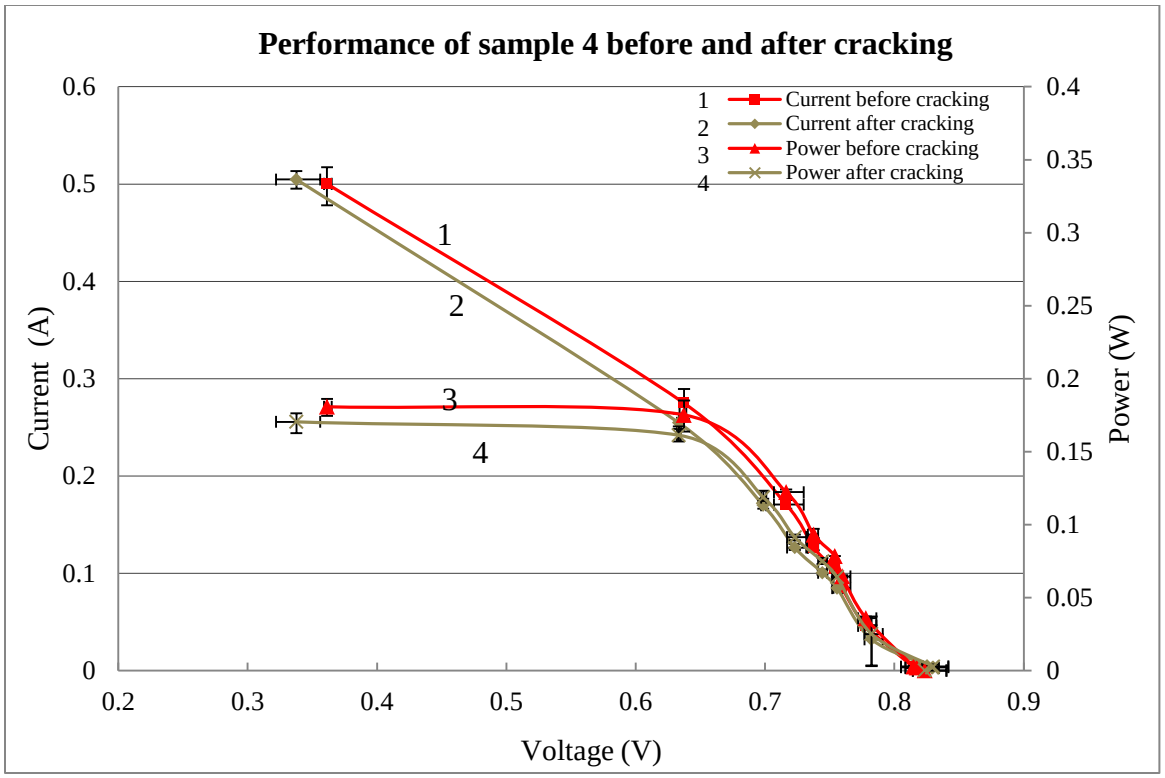

Figure 51. I-V curve of monocrystalline sample 4 before and after cracking.

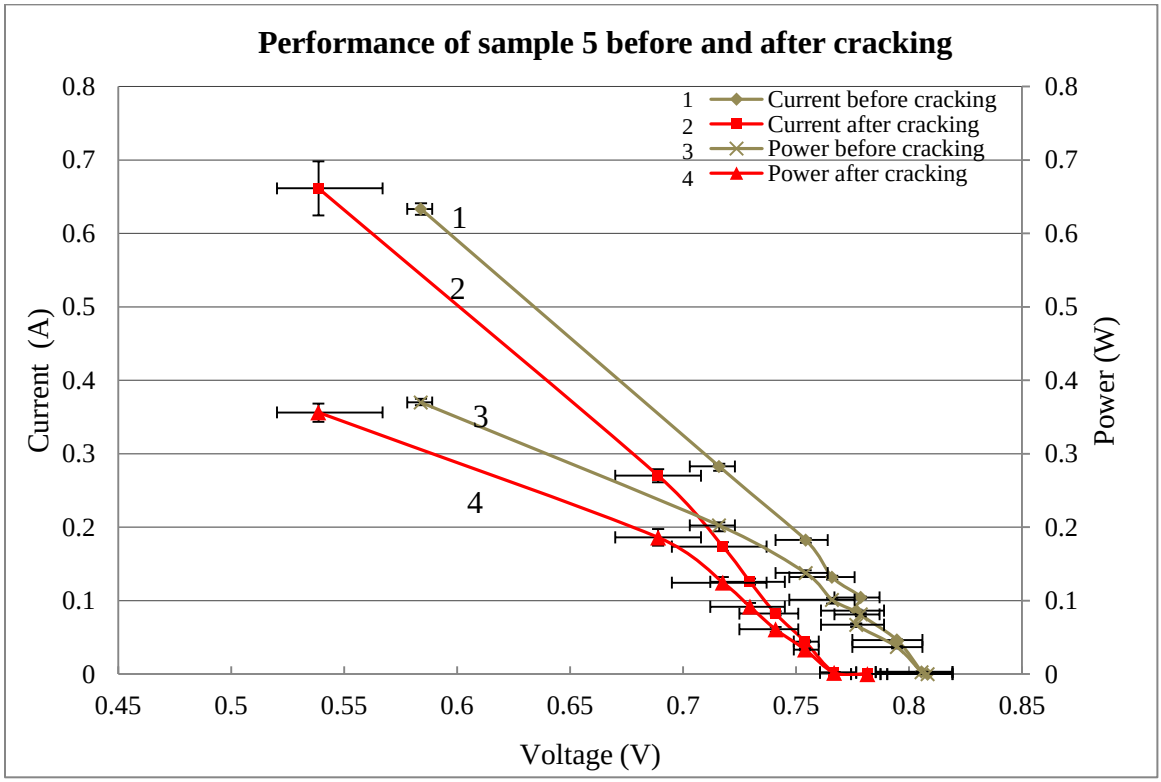

Figure 52. I-V curve of monocrystalline sample 5 before and after cracking.

The resulting efficiency and drop for each sample was calculated using [15] Equation 2 and summarized in the table below.

Table 3. Efficiency results for monocrystalline silicon solar cell samples.

Sample	Area (cm^2)	Efficiency before crack (%)	Efficiency deviation (%)	Efficiency after crack (%)	Efficiency deviation (%)	Efficiency reduction (%)
1	19.27	8.02	0.85	6.89	0.55	14.10
2	23.50	7.80	0.41	6.96	0.07	10.81
3	27.73	7.36	0.19	6.63	0.31	9.95
4	42.25	4.91	0.07	4.63	0.19	5.71
5	70.61	6.01	0.03	5.79	0.07	3.69

The following images correspond to SAM of polycrystalline samples before and after cracking. Some of the samples (Figure 53, Figure 56) were previously and unintentionally cracked but still cracks were induced to compare the drop in efficiency after cracking.

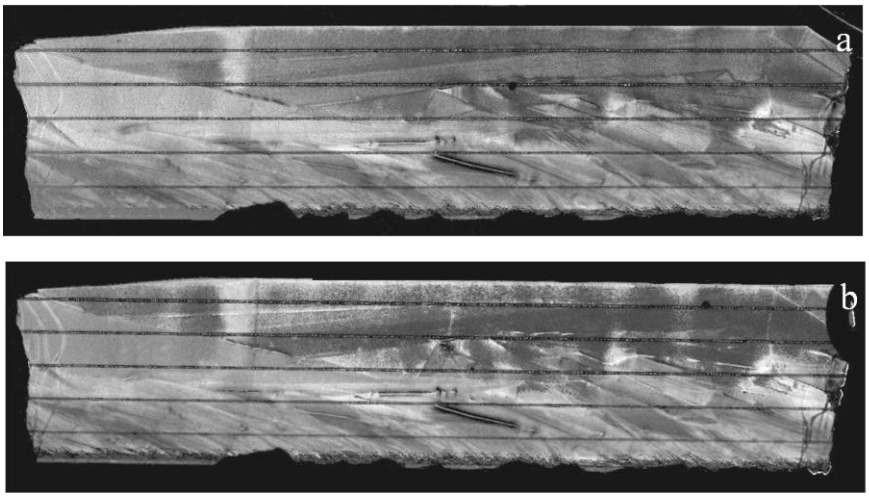

Figure 53. SAM of polycrystalline sample 1 (a) before and (b) after cracking.

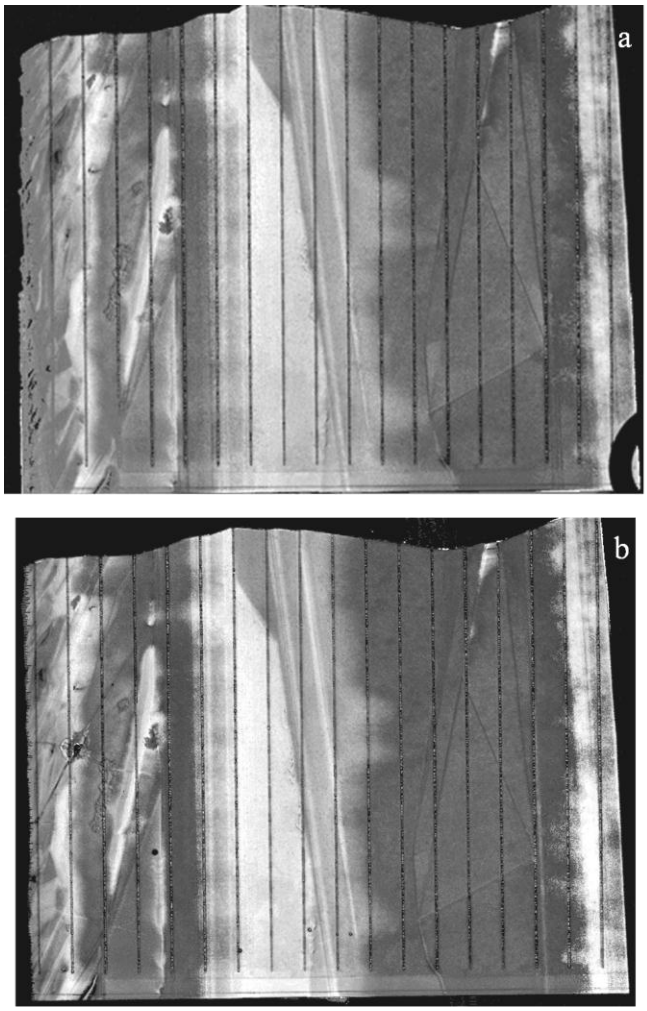

Figure 54. SAM of polycrystalline sample 2 (a) before and (b) after cracking.

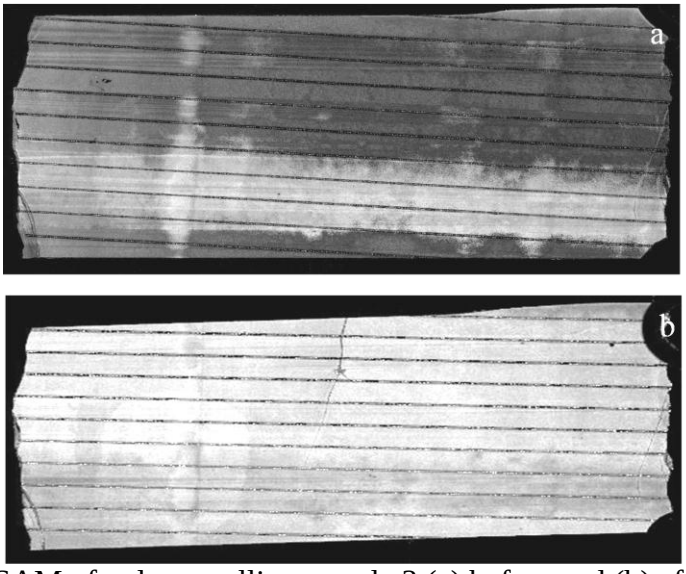

Figure 55. SAM of polycrystalline sample 3 (a) before and (b) after cracking.

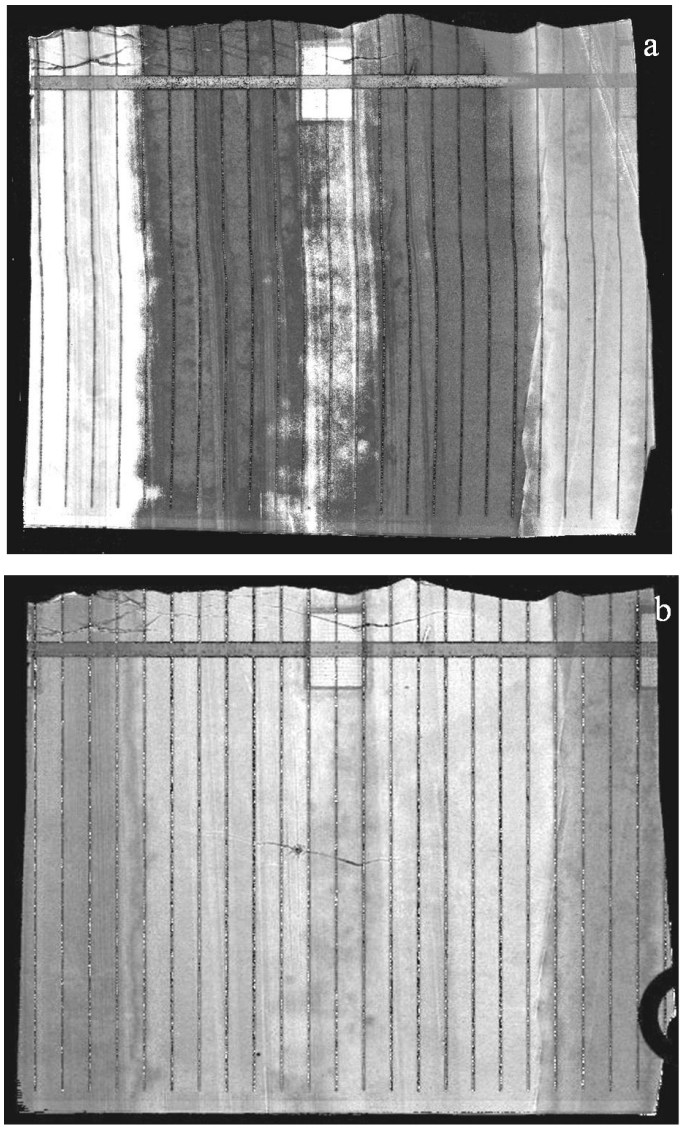

Figure 56. SAM of polycrystalline sample 4 (a) before and (b) after cracking.

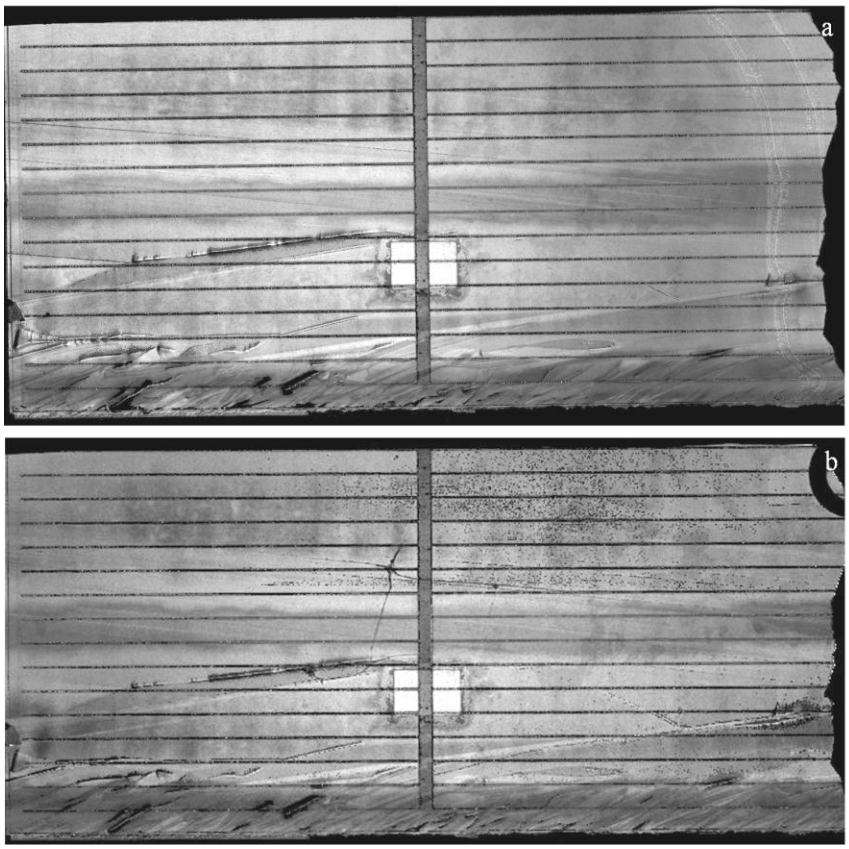

Figure 57. SAM of polycrystalline sample 5 (a) before and (b) after cracking.

The same measurement procedure as in the monocrystalline samples was followed in the polycrystalline samples. There were taken at least three measurements per each resistance value, incident radiation flux was simulated with light coming from an incandescent bulb at 3cm from the front surface of the cell sample. The following figures show the characteristic output of the polycrystalline samples before and after cracking for polycrystalline samples 1-5.

A clear difference in the characteristic parameters can be noticed in Figure 58 to Figure 62 while the shape of the curve is kept. Again, the shape of the curve does not match the real curve, this could be caused by the series and shunt resistances increment during the initial and subsequent breakage of the cells. Same behavior is shown in all samples.

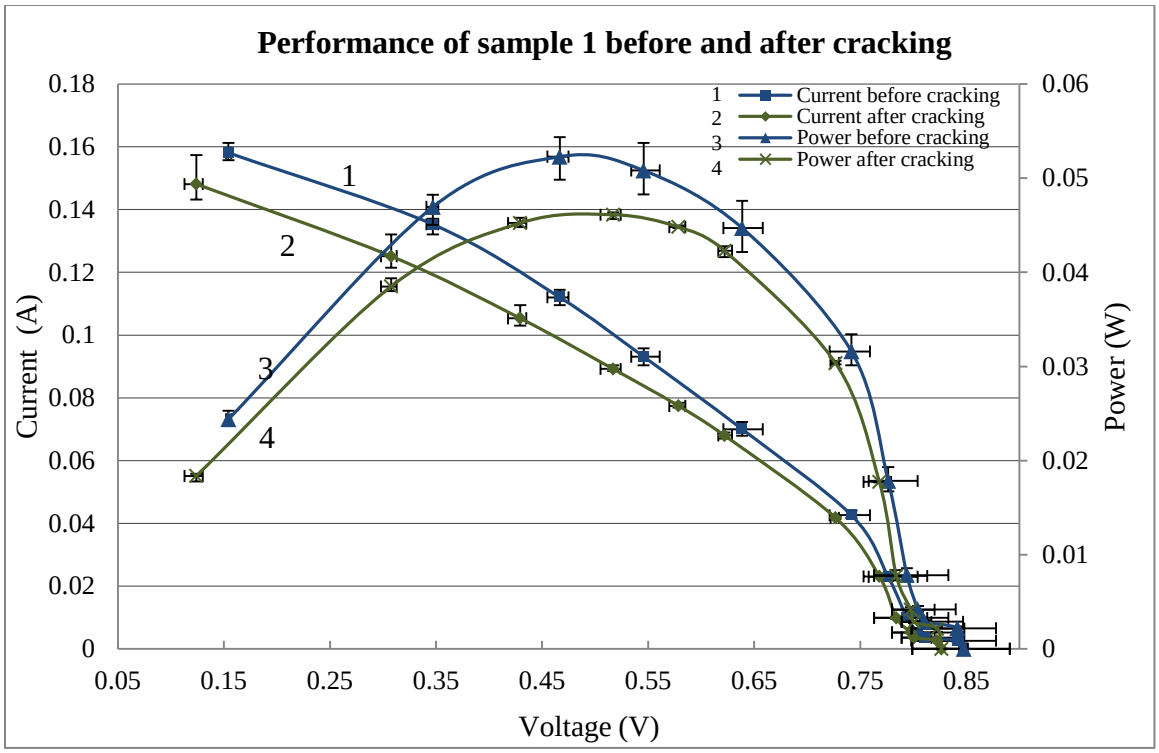

Figure 58. I-V curve of polycrystalline sample 1 before and after cracking.

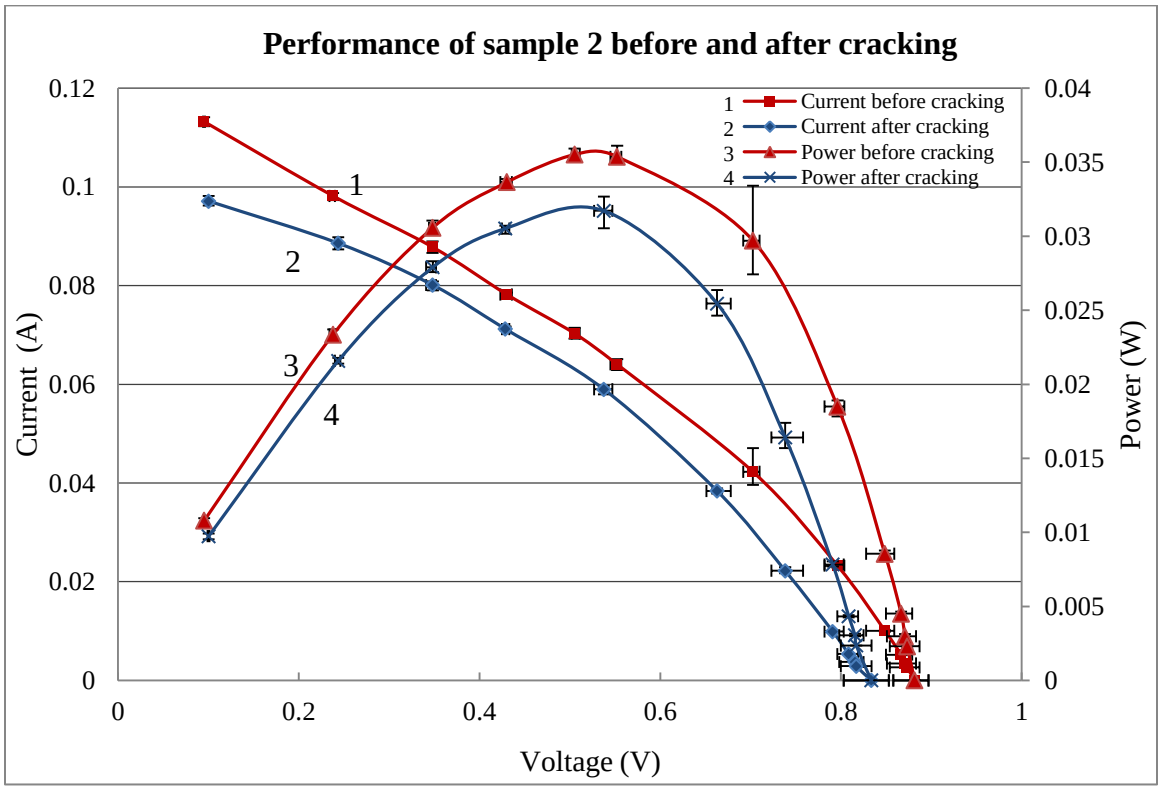

Figure 59. I-V curve of polycrystalline sample 2 before and after cracking.

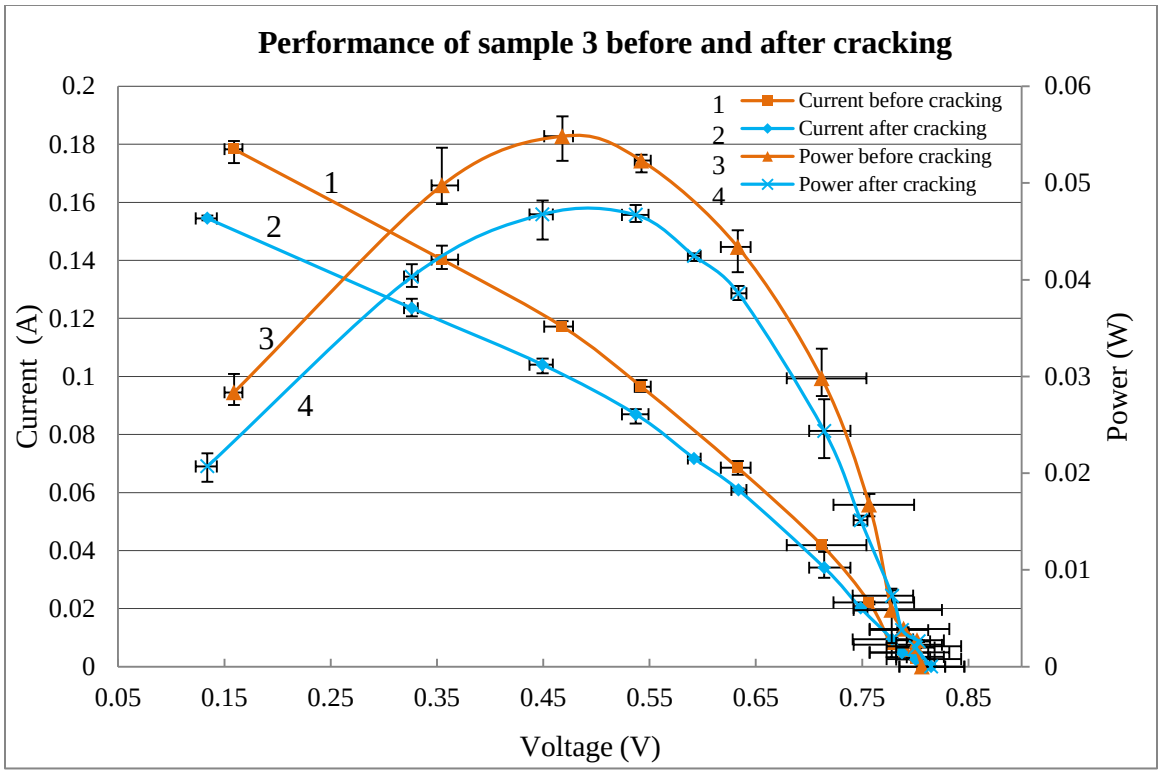

Figure 60. I-V curve of polycrystalline sample 3 before and after cracking.

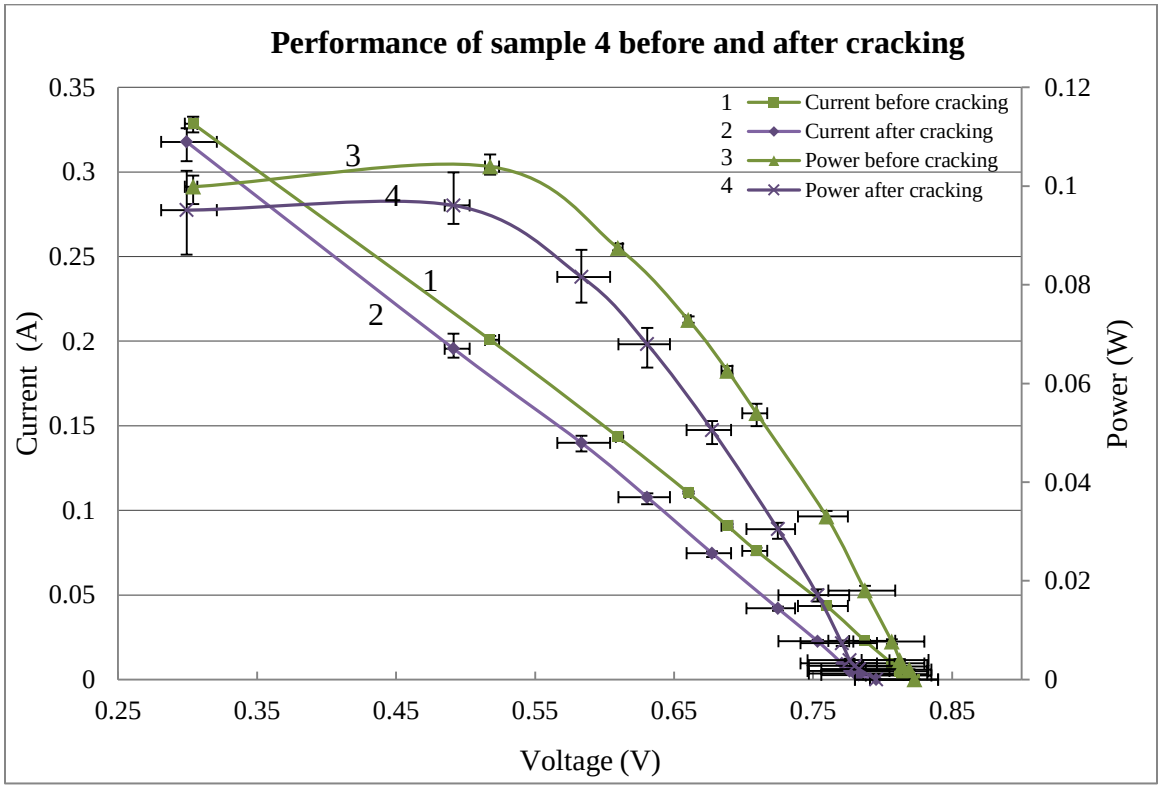

Figure 61. I-V curve of polycrystalline sample 4 before and after cracking.

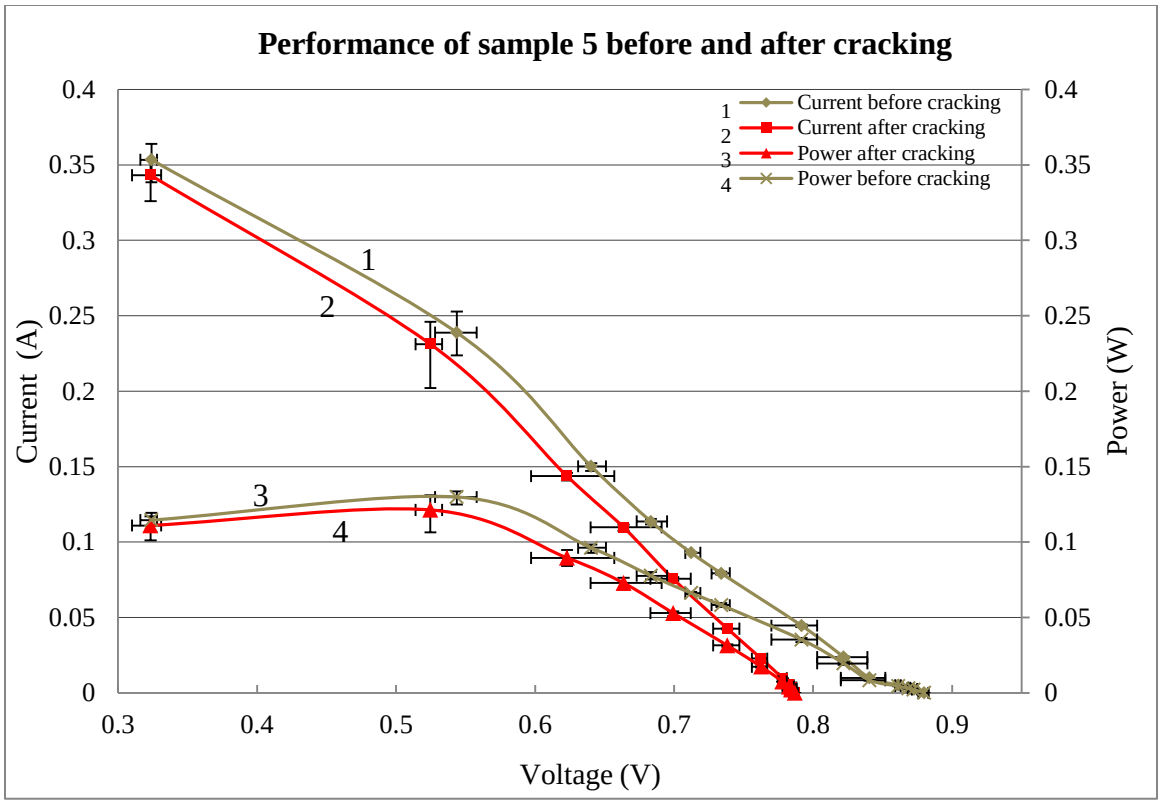

Figure 62. I-V curve of polycrystalline sample 5 before and after cracking.

The resulting efficiency and drop for each sample was calculated using Equation 2 and summarized in Table 4.

Table 4. Efficiency results for polycrystalline silicon solar cell samples.

Sample	Area (cm^2)	Efficiency before crack (%)	Efficiency deviation (%)	Efficiency after crack (%)	Efficiency deviation (%)	Efficiency reduction (%)
1	7.7	7.79	0.34	6.87	0.05	11.79
2	12.6	3.23	0.03	2.89	0.10	10.70
3	13.5	4.66	0.17	3.97	0.09	14.73
4	21.93	5.44	0.11	5.03	0.26	7.56
5	27.75	5.37	0.18	5.01	0.30	6.60

Chapter 4: Conclusions and Recommendations

The results reveal that SAM could be a reliable method of crack detection for silicon solar cells. The SAM technique relies on the difference in acoustic impedance at the ultrasound boundaries where cracks are usually shown in SAM images as black and defined lines. Cracks were analyzed in the single crystal and the polycrystalline silicon solar cells. A new approach was made using FIB cross section to confirm the existence of the crack in single crystal silicon cells, and to investigate the propagation of crack direction in solar cell. Monocrystalline cells showed a crack propagation direction corresponding to the preferred direction within the crystal. The FIB confirmed the cracks in polycrystalline silicon solar cells where these ribbon growth cells did not show a pattern in its propagation behavior.

Efficiency for both types of cells was calculated based on the current (I)- voltage (V) curves before and after the cracking of the cells. Some of the samples were cracked unintentionally, and a crack was induced intentionally to make a comparison between the efficiency drops in solar cell. The conversion efficiency values were estimated to be lower than the expected values which are obtained in solar cell. The values were well compared in chapter 3.

For monocrystalline samples the efficiency decreased in a higher percentage for low area samples. The efficiency reduction ranged between 3.69% for the biggest sample and 14.10% for the smallest sample. This could be explained by the fact that at more

active area, there are more carriers available and incident power from light to produce current in the cell.

Similar results were found at polycrystalline sample where the biggest sample showed the lowest efficiency reduction but in this case the smallest area did not show the highest efficiency reduction. Polycrystalline samples came from ribbon growth silicon, and some of the ribbons are long grains with different shapes and defects that could influence the amount of energy coming out of the cell. The efficiency reduction ranged from 6.6% for the biggest sample to 14.73%.

The findings reveal a high decrement in efficiency after cracks were induced; highlighting the importance of knowing the existence and location of the cracks. Despite the fact that the efficiency of monocrystalline samples is higher than in the polycrystalline samples, the drop is also higher; which could mean that cracks affect more single crystal cells than the polycrystalline version of the cells.

This research is the preliminary phase of a more controlled analysis of the influence of the cracks in the silicon solar cells. Improvements to reduce the errors in the measurements and control all the parameter involved are required. However, an enhanced set-up is highly recommended to keep the incident radiation in the highest peak of the solar cell emission spectra; as well as the use of a solar simulator. Furthermore, a controlled cracking process and measurements of the crack size are suggested. The use of complete cells of different sizes will extend and validate our results and diminish the influence of shunt and series resistances.

References

[1] K. Butti and J. Perlin, *A golden thread - 2500 years of solar architecture and technology*. London: Marion Boyars, 1980.

[2] Solar Energy International (SEI), "An Overview of Photovoltaics," in *Photovoltaics: Design and installation manual*.: New Society Publishers , 2004, ch. 1, pp. 2-4.

[3] T. Markwart and L. Castañer, "Principles of Solar Cell Operation," in *Solar Cells: Materials, Manufacture And Operation*, T. Markwart and L. Castañer, Eds. Oxford: Elsevier, 2005, ch. 2, pp. 19-26.

[4] Special materials research and technology, Inc. (2012, April) SPECMAT: Special materials research and technology, Inc. [Online]. http://specmat.com/Overview%20of%20Solar%20Cells.html

[5] J. Szlufcik, G. Agostinelli, F. Duerinck, G. Beaucarne , and E. Van Kerschaver, "Low cost industrial technologies of crystalline silicon solar cells," in *Solar cells: Materials, manufacture and operation*, T. Markvart and L. Castañer, Eds. Oxford: Elsevier, 2005, ch. 2, pp. 90-110.

[6] Stephenson & Associates, Inc. (2012, October) Fundamental properties of solar cells and pastes for silicon solar cells. Document. [Online]. http://stephenson-associates-inc.com/Fundamental%20Properties%20of%20Silicon%20Solar%20Cells%20and%20Pastes.pdf

[7] O. Von Roos, "A simple theory of back surface field (BSF) solar cells," *Journal in applied physics*, vol. 49, no. 6, pp. 3503-3511, June 1978.

[8] V. A. Popovich, M. Janssen, I. M. Richardson, T. Van Amste, and I. J. Bennett, "Microstructure and mechanical properties of aluminum back contact layers," *Solar energy materials and solar cells*, no. 95, pp. 93-96, April 2011.

[9] J. L. Gray, "Physics of the solar cell," in *Handbook of photovoltaic science and engineering*, A. Luque and S. Hegedeus, Eds. Oxford, UK: Wiley, 2003, ch. 3, pp. 61-112.

[10] Enerpoint. (2012, September) Enerpoint: Your solar link. [Online]. http://www.enerpoint.net/photovoltaic_technology_2.php

[11] T. Kilper et al., "Oxygen and nitrogen impurities in microcrystalline silicon deposited under optimized conditions: Influence on material properties and solar cell performance," *Journal of applied physics*, vol. 105, 2009.

[12] A. Cheknane, B. Benyoucef, and A. Chaker, "Performance of concentrator solar cells with passive cooling," *Semiconductor science and technology*, vol. 21, no. 2, 2006.

[13] X. Han, Y. Wang, L. Zhu, H. Xiang, and H. Zhang, "Mechanism study of the electrical performance change of silicon concentrator solar cells immersed in de-ionized water," *Energy conversion and management*, vol. 53, no. 1, pp. 1-10, 2012.

[14] M. J. Morgan, G. Jakovidis, and I. McLeod. (1995) An experiment to measure the I-Vcharacteristics of a silicon solar cell. Document.

[15] G. L. Araujo, "The solar cell," in *Solar electricity: engineering of photovoltaic systems*, E. Lorenzo, Ed. Sevilla, Espana: Progensa, 1994, ch. 2, pp. 59-85.

[16] G. M. Masters, *Renewable and efficienct electric power systems*. New jersey, United States of America: John Wiley and Sons, 2004.

[17] Keithley Instruments Inc., Measuring photovoltaic cell I-V characteristics with the model 2420 sourcemeter instrument, 2003, Application note series.

[18] M. Wolf and H. Rauschenbach, "Series resistance effect on solar cell measurements," *Advanced energy conversion*, vol. 3, pp. 455-479, 1963.

[19] T. J. McMahon, T. S. Basso, and S. R. Rummel , "Cell shunt resistance and photovoltaic module performance," in *Photovoltaic Specialists Conference, Conference Record of the Twenty Fifth IEEE*, Washington, DC, 1996, pp. 1291-1294.

[20] F. Khan, S. Singh, S. N. Singh, and M. Husain, "Effect of illumination intensity on cell parameters of a silicon solar cell," *Solar energy materials and solar cells*, no. 94, pp. 1473–1476, April 2010.

[21] R. O. Ritchie, "Failure of silicon: Crack formation and propagation," in *13th Workshop on Crystalline solar cell materials and processes*, Vail, CO, 2003.

[22] V. A. Popovich, A. Yunus, M. Janssen, I. M. Richardson, and I. J. Bennett, "Effect of silicon solar cell processing parameters and crystallinity on mechanical strength," *Solar Energy Materials & Solar Cells*, no. 95, pp. 97-100, 2011.

[23] P. S. Raghavan, Y. Wan, and C. P. Khattak, "Crack detection in photovoltaic quality control," in *16th Workshop on Crystalline silicon solar cells and modules: Materials and processes. NREL.*, Denver, CO, 2006, pp. 125-128.

[24] M. Köntges, I. Kunze, S. Kajari-Schröder, X. Breitenmoser, and B. Bjørneklett, "The risk of power loss in crystalline silicon based photovoltaic modules due to microcracks," *Solar energy materials and solar cells*, no. 95, pp. 1131-1137, 2011.

[25] M. Köntges, I. Kunze, S. Kajari-Schröder, X. Breitenmoser, and B. Bjørneklett, Origin and consequences of micro-cracks in crystalline silicon solar modules, 2011.

[26] Fahhad Alharbi, John D. Bass, Abdelmajid Salhi, Ho-Cheol Kimb, and Robert D. Miller, "Abundant non-toxic materials for thin film solar cells: Alternative to conventional materials.," *Renewable Energy*, vol. 36, no. 10, pp. 2753-2758, 2011.

[27] H. Moreno-Garcia, M. T. S. Nair, and P. K. Nair, "Chemically deposited lead sulfide and bismuth sulfide thin films and bismuth sulfide thin films and Bi2Si3/PbS solar cells," *Thin solid films*, vol. 519, no. 7, pp. 2287-2295, 2011.

[28] S. E. Shaheen, D. S. Ginley, and G. E. Jabbour, "Organic based photovoltaics: Toward low-cost power generation," *MRS Bulletin*, vol. 30, pp. 10-19, 2005.

[29] T. Gorbach, V. Kostylyov, and P. Smertenko, "New organic materials for organic-inorganic silicon-based solar cells," *Molecular Crystals & Liquid Crystals*, vol. 535, pp. 174-178, 2011.

[30] R. Janssen. Introduction to polymer solar cells. [Online]. http://user.chem.tue.nl/janssen/SolarCells/Polymer%20solar%20cells.pdf

[31] A. Monastyrskyi, S. Ostapenko, O. Polupan, H. Maeckel, and M. A. Vazquez, "Resonance Ultrasonic Vibrations for in-line crack detection in silicon wafers and solar cells," in *Photovoltaic Specialists Conference*, San Diego, CA, USA, 2008.

[32] A. Goetzberger, J. Knobloch, and B. VoB, "Si Solar Cell Technology," in *Crystalline Silicon Solar Cells*.: John Wiley & Sons, 1998, pp. 133-162.

[33] I. Tarasov, *Defect diagnostic using scanning photoluminescence in multicrystalline silicon for solar cells*. Tampa, Fl: University of South Florida, 2002.

[34] F. Ferrazza, "Crystalline silicon: Manufacture and properties," in *Solar Cells: Materials, Manufacture And Operation*. Oxford, UK: Elsevier, 2005, pp. 72-87.

[35] W. Koch et al., "Bulk Crystal Growth and Wafering for PV," in *Handbook of photovoltaic science and engineering*, A. Luque and S. Hegedeus, Eds. Chichester, UK: Wiley, 2003, ch. 6, pp. 205-254.

[36] K. Davami, M. K. Besharati, and M. Shaygan, "Modeling of Solidification Conditions and Melt treatment on microporosiy formation," *International journal of mathematics and computers in simulation*, vol. 2, no. 2, pp. 144-151, 2008.

[37] M. A. Green, "Crystalline and thin-film silicon solar cells: state of the art and future potential," *Solar Energy*, vol. 74, no. 3, pp. 181–192, March 2003.

[38] E. A. Schiff and X. Deng, "Amorphous silicon–based solar cells," in *Handbook of photovoltaic science and engineering*, A. Luque and S. Hegedeus , Eds. Oxford, UK: Wiley, 2003, ch. 12, pp. 505-566.

[39] A. Belyaev, O. Polupan, W. Dallas, S. Ostapenko, and D. Hess, "Crack detection and analyses using resonance ultrasonic vibrations in full size crystalline silicon wafers," *Applied physics letters*, vol. 88, 2006.

[40] W. Dallas, O. Polupan, and S. Ostapenko, "Resonance ultrasonic vibrations for crack detection in photovoltaic silicon wafers," *Measurement science and technology*, vol. 18, pp. 852-858, 2007.

[41] A. Belyaev, O. Polupan, S. Ostapenko, S. Hess, and J. P. Kalejs, "Resonance ultrasonic vibration diagnostics of elastic stress in full-size silicon wafers," *Semiconductor science technology*, vol. 21, pp. 254-260, 2006.

[42] H. Wu et al., "Effect of handling stress on resonance ultrasonic vibrations in thin silicon wafers," in *35th IEEE Photovoltaic Specialists Conference*, Honolulu, Hawaii, 2010.

[43] Yu. Emirov et al., "Pinhole detection in Si solar cells usingg resonance ultrasonic vibrations," in *37th IEEE Photovoltaic Specialists Conference*, Seattle, Washington, 2011.

[44] Y. Emirov et al., "In-line crack inspection and process control in solar and fuel cells using resonance ultrasonic vibrations," in *2012 MRS spring meeting and exhibit*, San Francisco, 2012.

[45] J. Yang, "Non-destructive identification of defects in integrated circuit packages by scanning acoustic microscopy," *Microelectronics reliability*, vol. 36, no. 9, pp. 1291-1295, 1996.

[46] Learner corner: SONIX, Inc. [Online]. http://www.sonix.com/learning/ultrasonics.php3

[47] Z. Connor , M. Fine, M. Seniw, and J. Achenbach, "Using scanning acoustic microscopy to study subsurface defects and crack propagation in materials," *JOM:Journal of the minerals, metals and materials society (TMS)*, vol. 50, no. 11, 1998.

[48] S. Gao and J. Kim, "Scanning acoustic microscopy as a tool for quantitative characterisation of damage in CFRPs," *Composites science and technology*, no. 59, pp. 345-354, 1999.

[49] B. True. Photoluminescence and electroluminescence for silicon solar cells. [Online]. http://www.laser2000.de/fileadmin/kataloge/INTEVAC_SolarCellWhitePaper_BruceTrue.pdf

[50] S. Johnston and NREL National renewable energy laboratory. (2012, February) Photoluminescence and electroluminescence imaging workstation. [Online]. http://www.nrel.gov/pv/pdil/samc_photoluminescence.html

[51] J. Lu, G. Rozgonyi, L. Kordas, and T. Ciszek, "Investigation of electrical activity of dislocation and grain boundary in polycrystalline float zone silicon," in *National center for photovoltaics and solar program review meeting*, Denver, Colorado, 2003.

[52] T. Trupke et al., "Photoluminescence imaging for photovoltaic applications," *Energy Procedia*, vol. 15, pp. 135 – 146, 2012.

[53] B. Hoex, W Zhang, and A. G. Aberle, "Advanced Characterisation of Silicon Wafer Solar Cells," *Energy Procedia*, vol. 15, pp. 147 – 154, 2012.

[54] A. Monastyrskyi, Resonance ultrasonic vibrations and photoluminescence mapping for crack detection in crystalline silicon wafers and solar cells, 2008.

[55] T. Trupke, R. A. Bardos, M. C. Schubert, and W. Warta, "Photoluminescence imaging of silicon wafers," *Applied Physics Letters*, vol. 89, no. 4, 2006.

[56] W. Dallas, Resonance ultrasonic vibrations (RUV) for crack detetion in silicon wafers for solar cells, 2006.

[57] J. Rantala, D. Wu, A. Salerno, and G. Busse, "Lock-in thermography with mechanical loss angle heating at ultrasonic frequencies," *NDTnet*, vol. 2, no. 3, March 1997.

[58] A. Dillenza, G. Bussea, and D. Wub, "Ultrasound lock-in thermography: feasibilities and limitations," in *SPIE conference*, Stuttgart, Germany, 1999.

[59] C. Meola, G. Carlomagno, A. Squillace , and A. Vitiello, "Non-destructive evaluation of aerospace materials with lock-in thermography," *Engineering Failure Analysis*, no. 13, pp. 380-388, 2006.

[60] Y. Leng, "Scanning electron microscopy," in *Materials characterization: Introduction to microscopic and spectroscopic methods*. Singapore: JohnWiley & Sons (Asia) Pte Ltd, 2008, pp. 121-144.

[61] P. W. Hawkes, "The scanning electron microscope and its field of application," in *Advances in Imaging and Electron Physics*. San Diego: Elsevier Inc., 2004, pp. 111-125.

[62] L. A. Giannuzzi and F. A. Stevie, Eds., *Introduction to focused ion beams: Instrumentacion, theory, techniques and practice.* New york, United States of America: Springer Science, 2005.

[63] FEI Company. (2005) Focused ion beam technology, capabilities and applications. [Online]. http://www.fei.com/uploadedFiles/Documents/Content/2006_06_FIB_Overview_pb.pdf

[64] S. Ostapenko, I. Tarasov, J. P. Kalejs, C. Haessler, and E. U. Reisner, "Defect monitoring using scanning photoluminescence spectroscopy in multicrystalline silicon wafers," *Semiconductor science technology*, no. 15, pp. 840–848, June 2000.

Appendices

Appendix A Copyright and Permissions

A.1 Permission to Reproduce Figure 7

The following letters show the permission to reproduce Figure 1 of "Resonance ultrasonic vibration diagnostics of elastic stress in full-size silicon wafers" by A. Belyaev, O. Polupan, S. Ostapenko, S. Hess, and J. P. Kalejs, Semiconductor science technology, vol. 21, pp. 254-260, 2006 (IOP); which corresponds to Figure 7 in this thesis.

To: permissions <permissions@iop.org>,
Cc:
Bcc:
Subject: Permission request form2-Paper from Semiconductor Science Technology
From: Maria Echeverria Molina <miecheverria@mail.usf.edu> - Saturday 03/11/2012 05:06

1 attachment

Permission request form-fig 1 in Resonance ultrasonic vibration diagnostics of elastic stress in full-size silicon wafers.docx

Hello.

I am graduate student of University of South Florida 4202 E. Fowler Avenue Tampa, FL 33620. I am preparing my Master's thesis titled "Cracks analysis in Silicon solar cells" and I would like to get permission to publish Figure 1 of "Resonance ultrasonic vibration diagnostics of elastic stress in full-size silicon wafers" by A. Belyaev, O. Polupan, S. Ostapenko, S. Hess, and J. P. Kalejs, *Semiconductor science technology,* vol. 21, pp. 254-260, 2006 (IOP).

This figure would be presented in Chapter 1: Introduction and Background of my Master's Thesis.
I will really appreciate your prompt attention to this request.
I am attaching a letter requesting the permission.
Thanks and bests,

--

Maria I Echeverria
Materials Science and Engineering MS Student
Mechanical Engineering Department
University of South Florida

(813)-3179628

Appendix A (Continued)

11/02/2012

To whom it may concern

I am preparing my Master's Thesis entitled "Crack Analysis in Silicon Solar Cells" to be published in University of South Florida 4202 E. Fowler Avenue Tampa, FL 33620.

I would appreciate permission to reproduce the following item(s) in both print and electronic editions of my Master's Thesis and derivative products and in publisher authorized distribution by third party distributors, aggregators and other licensees such as abstracting and indexing services. I should be grateful for nonexclusive perpetual world rights in all languages and media. Unless you indicate otherwise, I will use the complete reference given below as the credit line.

In case you do not control these rights, I would appreciate it if you could let me know to whom I should apply for permissions.

✓ Figure 1 of "Resonance ultrasonic vibration diagnostics of elastic stress in full-size silicon wafers" by A. Belyaev, O. Polupan, S. Ostapenko, S. Hess, and J. P. Kalejs, *Semiconductor science technology,* vol. 21, pp. 254-260, 2006 (IOP).

The figure would be presented in Chapter 1 of my document, which corresponds to Introduction and Background.

For your convenience a copy of this letter may serve as a release form: the duplicate copy may be retained for your files.

Thank you for your prompt attention to this request.

Yours sincerely

Maria I. Echeverria Molina

I/We grant permission for the use of the work as set out above.

Signed:

Date:

On behalf of Publisher:

Appendix A (Continued)

PERMISSION TO REPRODUCE AS REQUESTED IS GIVEN PROVIDED THAT:

(a) the consent of the author(s) is obtained
(b) the source of the material including author, title of article, title of journal, volume number, issue number (if relevant), page range (or first page if this is the only information available), date and publisher is acknowledged.
(c) for material being published electronically, a link back to the original article should be provided (via DOI).

IOP Publishing Ltd
Temple Circus
Temple Way
BRISTOL
BS1 6BE

05/11/2012
Date

Sarah Ryder
Rights & Permissions

A.2 Permission to Reproduce Figure 8

The following letters show the permission to reproduce Figure 8 of "Resonance ultrasonic vibrations for crack detection in photovoltaic silicon wafers" by W. Dallas, O. Polupan, and S. Ostapenko, Measurement science and technology, vol. 18, pp. 852-858, 2007 (IOP); which corresponds to Figure 8 in this thesis.

Appendix A (Continued)

To: permissions@iop.org,
Cc:
Bcc:
Subject: Permission request form3-Paper from Measurement science and technology
From: Maria Echeverria Molina <miecheverria@mail.usf.edu> - Saturday 03/11/2012 05:24

1 attachment

Permission request form-fig 8 in Resonance ultrasonic vibrations for crack detection in photovoltaic silicon wafers.docx

Hello.
I am graduate student of University of South Florida 4202 E. Fowler Avenue Tampa, FL 33620. I am preparing my Master's thesis titled "Cracks analysis in Silicon solar cells" and I would like to get permission to publish Figure 8 of "Resonance ultrasonic vibrations for crack detection in photovoltaic silicon wafers" by W. Dallas, O. Polupan, and S. Ostapenko, *Measurement science and technology* , vol. 18, pp. 852-858, 2007 (IOP).

This figure would be presented in Chapter 1: Introduction and Background of my Master's Thesis.
I will really appreciate your prompt attention to this request.
I am attaching a letter requesting the permission.
Thanks and bests,
--
Maria I Echeverria
Materials Science and Engineering MS Student
Mechanical Engineering Department
University of South Florida

(813)-3179628

Appendix A (Continued)

11/02/2012

To whom it may concern

I am preparing my Master's Thesis entitled "Crack Analysis in Silicon Solar Cells" to be published in University of South Florida 4202 E. Fowler Avenue Tampa, FL 33620.

I would appreciate permission to reproduce the following item(s) in both print and electronic editions of my Master's Thesis and derivative products and in publisher authorized distribution by third party distributors, aggregators and other licensees such as abstracting and indexing services. I should be grateful for nonexclusive perpetual world rights in all languages and media. Unless you indicate otherwise, I will use the complete reference given below as the credit line.

In case you do not control these rights, I would appreciate it if you could let me know to whom I should apply for permissions.

✓ Figure 8 of "Resonance ultrasonic vibrations for crack detection in photovoltaic silicon wafers" by W. Dallas, O. Polupan, and S. Ostapenko, *Measurement science and technology*, vol. 18, pp. 852-858, 2007 (IOP).

The figure would be presented in Chapter 1 of my document, which corresponds to Introduction and Background.

For your convenience a copy of this letter may serve as a release form: the duplicate copy may be retained for your files.

Thank you for your prompt attention to this request.

Yours sincerely

Maria I. Echeverria Molina

I/We grant permission for the use of the work as set out above.

Signed:

Date:

On behalf of Publisher:

Appendix A (Continued)

PERMISSION TO REPRODUCE AS REQUESTED IS GIVEN PROVIDED THAT:

(a) the consent of the author(s) is obtained
(b) the source of the material including author, title of article, title of journal, volume number, issue number (if relevant), page range (or first page if this is the only information available), date and publisher is acknowledged.
(c) for material being published electronically, a link back to the original article should be provided (via DOI).

IOP Publishing Ltd
Temple Circus
Temple Way
BRISTOL
BS1 6BE

05/11/2012
Date

Swan Rahr
Rights & Permissions